Article

Cell Host & Microbe

# Metatranscriptomics uncovers diurnal functional shifts in bacterial transgenes with profound metabolic effects

## Graphical abstract

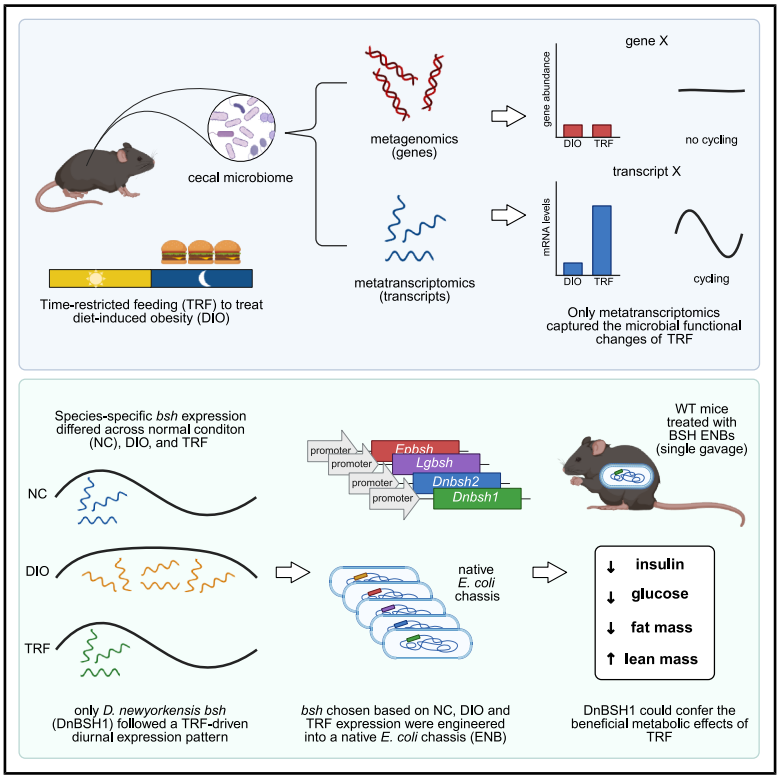


## Highlights

- Metatranscriptomics reveals diurnal functional shifts missed by metagenomics
- Time-restricted feeding (TRF) restores microbial transcript cycling under high-fat diet
- *D. newyorkensis bsh1* (DnBSH1) exhibits unique diurnal expression under TRF conditions
- Administration of *E. coli* engineered to express DnBSH1 improves mouse metabolic health

## Authors

Stephany Flores Ramos, Nicole Siguenza, Wuling Zhong, ..., Satchidananda Panda, Rob Knight, Amir Zarrinpar

## Correspondence

azarrinpar@ucsd.edu

## In brief

Flores Ramos et al. use metatranscriptomics to reveal diurnal functional shifts in microbes under time-restricted feeding, identifying a *Dubosiella newyorkensis* bile salt hydrolase (DnBSH1) with time-dependent expression. Engineering DnBSH1 into *E. coli* improves glucose metabolism and reduces body fat in mice, highlighting the promise of metatranscriptomics in bacterial gene discovery.

Flores Ramos et al., 2025, Cell Host & Microbe *33*, 1057–1072
July 9, 2025 Published by Elsevier Inc.
https://doi.org/10.1016/j.chom.2025.05.024

CellPress

Cell Host & Microbe

CellPress

Article

# Metatranscriptomics uncovers diurnal functional shifts in bacterial transgenes with profound metabolic effects

Stephany Flores Ramos,[1,2,3] Nicole Siguenza,[1,2] Wuling Zhong,[1] Ipsita Mohanty,[4] Amulya Lingaraju,[1] R. Alexander Richter,[1] Smruthi Karthikeyan,[3,6] April L. Lukowski,[4,7] Qiyun Zhu,[8,9] Wilhan D.G. Nunes,[4,5] Jasmine Zemlin,[4] Zhenjiang Zech Xu,[3,10] Jeff Hasty,[12,13,15] Pieter C. Dorrestein,[3,4,5] Satchidananda Panda,[11] Rob Knight,[2,3,12,13,14,15,16] and Amir Zarrinpar[1,2,12,13,15,17,18,19,20,*]

[1]Division of Gastroenterology, University of California, San Diego, La Jolla, CA, USA
[2]Biomedical Sciences Graduate Program, University of California, San Diego, La Jolla, CA, USA
[3]Department of Pediatrics, University of California, San Diego, La Jolla, CA, USA
[4]Skaggs School of Pharmacy and Pharmaceutical Sciences, University of California, San Diego, La Jolla, CA, USA
[5]Collaborative Mass Spectrometry Innovation Center, Skaggs School of Pharmacy and Pharmaceutical Sciences, University of California, San Diego, La Jolla, CA, USA
[6]Division of Engineering and Applied Science, California Institute of Technology, Pasadena, CA, USA
[7]Scripps Institution of Oceanography, University of California, San Diego, La Jolla, CA, USA
[8]School of Life Sciences, Arizona State University, Tempe, AZ, USA
[9]Biodesign Center for Fundamental and Applied Microbiomics, Arizona State University, Tempe, AZ, USA
[10]Key Laboratory of Food Science and Technology, Nanchang University, Nanchang, China
[11]Salk Institute for Biological Studies, La Jolla, CA, USA
[12]Shu Chien-Gene Lay Department of Bioengineering, University of California, San Diego, La Jolla, CA, USA
[13]Center for Microbiome Innovation, University of California, San Diego, La Jolla, CA, USA
[14]Department of Computer Science and Engineering, University of California, San Diego, La Jolla, CA, USA
[15]Synthetic Biology Institute, University of California, San Diego, La Jolla, CA, USA
[16]Halıcıoğlu Data Science Institute, University of California, San Diego, La Jolla, CA, USA
[17]Moores Cancer Center, University of California, San Diego, La Jolla, CA, USA
[18]Division of Gastroenterology, Jennifer Moreno Department of Veterans Affairs Medical Center, La Jolla, CA, USA
[19]Institute of Diabetes and Metabolic Health, University of California, San Diego, La Jolla, CA, USA
[20]Lead contact
*Correspondence: azarrinpar@ucsd.edu
https://doi.org/10.1016/j.chom.2025.05.024

## SUMMARY

Diurnal rhythmicity in the gut maintains gut integrity, circadian rhythms, and metabolic homeostasis. However, existing studies focus on microbial composition rather than transcriptional activity. To understand microbial functional dynamics, we characterize diurnal fluctuations in the mouse cecal metatranscriptome and metagenome under high-fat diet and time-restricted feeding (TRF). We show that metatranscriptomics uncovers TRF-induced time-dependent microbial functional shifts that are undetectable with metagenomics alone. We also found bile salt hydrolase (*bsh*) from *Dubosiella newyorkensis* exhibits diurnal expression in the TRF group. Engineering this *bsh*, along with other candidates, into a native *E. coli* chassis reveals distinct differences in deconjugation and amidation activities, underscoring functional specificity. *In vivo*, a *D. newyorkensis bsh* improves insulin sensitivity, glucose tolerance, and body composition, suggesting a direct role in TRF metabolic benefits. This study highlights how coupling metatranscriptomics with engineered bacterial systems is a powerful approach for uncovering time-dependent bacterial functions related to health and disease.

## INTRODUCTION

The healthy gut microbiome is dynamic, exhibiting oscillations in microbial populations over a diurnal cycle.[1–4] Disruptions to these patterns—such as those caused by xenobiotics or a high-fat diet (HFD)[1–5]—contribute to metabolic dysfunction. Time-restricted feeding (TRF), a behavioral strategy that limits food access to specific periods aligned with the circadian cycle, has emerged as a promising intervention to restore rhythmicity. In mice, TRF mitigates HFD-induced insulin resistance, adiposity, and inflammation while also realigning circadian gene expression and bile acid (BA) metabolism.[1,3,6–9]

TRF restores diurnal oscillations in bile salt hydrolase (BSH)-mediated BA deconjugation, a microbial activity associated with improved host metabolic outcomes.[3,10,11] Despite these changes, TRF only partially restores microbial cycling compared with normal chow diet (NCD) conditions.[1,3] This disconnect suggests that compositional data alone—typically assessed by 16S rRNA or metagenomic sequencing—are insufficient to capture the dynamic functional landscape of the microbiome.

Metatranscriptomics is the study of the transcriptional profile of a microbial community.[12] It offers a more direct view of microbial activity by profiling RNA transcripts, which reflect real-time functional states.[13,14] With short half-lives and high responsiveness to environmental cues,[5,15–17] transcripts enable detection of rapid microbiome shifts that are often missed by DNA-based methods. Metatranscriptomics can reveal functionally active pathways in microbial communities[16,18] in diseases such as inflammatory bowel disease (IBD),[19] obesity,[20] cancer,[21] and type 1 (T1D) and type 2 diabetes (T2D)[22] and lead to the discovery of new microbial functions, such as a bacterial catechol dehydrogenase.[23] Despite its potential, metatranscriptomics has rarely been used to guide the development of live bacterial therapeutics (LBTs), largely because the functional hypotheses it generates are often difficult to test experimentally, representing a missed opportunity to functionally link microbial gene expression with host metabolic outcomes.

To understand the functional activity of microbes under TRF, we used metatranscriptomics and metagenomics to profile microbial activity in the cecum of diet-induced obese (DIO) mice under *ad libitum* or TRF conditions across a 24-h cycle. Given the temporal sensitivity of metatranscriptomics, we hypothesized that it would reveal time-dependent microbial functions driven by TRF. Our goal was to identify TRF-responsive microbial functions and test their therapeutic relevance by engineering candidate genes into a native *Escherichia coli* chassis. This study demonstrates that metatranscriptomics can uncover time-dependent microbial activities and directly inform the development of function-based microbial therapeutics.

## RESULTS

### Metatranscriptomics captures functional dynamics driven by diet and feeding behavior

To understand the impact of diet and feeding behavior on microbial functions, we subjected 8-week-old wild-type male C57BL/6 mice to different diets and food access patterns as previously described.[1] Briefly, mice were divided into three groups based on the following diet/feeding conditions: (1) NCD with *ad libitum* food access (NA; $n = 18$), (2) HFD with *ad libitum* food access (FA; $n = 18$), and (3) HFD under 8-h TRF from Zeitgeber time (ZT) 13 to 21 (FT; $n = 18$) (Figure 1A). After 8 weeks on these regimens, metabolic phenotyping confirmed that FT mice were protected from HFD-induced metabolic dysfunction (Figures S1A and S1B).[1] Whole-cecal contents were collected every 4 h over a 24-h period (ZT1, 5, 9, 13, 17, and 21; $n = 3$ mice/time point/condition) to characterize diurnal microbial activity.

We first analyzed α-diversity across all conditions and omics methods (16S, metagenomics, and metatranscriptomics) without considering time of collection. No significant differences were observed in microbial composition (16S; one-way ANOVA, $p = 0.80$) or genes/functional potential (metagenomics; $p = 0.26$) across diet and feeding patterns (Figure S1C). By contrast, transcript-level α-diversity (metatranscriptomics) differed significantly between conditions ($p < 0.001$), particularly between NA and both HFD groups (Mann-Whitney U test, NA vs. FA: $p < 0.001$; NA vs. FT: $p < 0.001$). When time points were analyzed individually, α-diversity differences emerged at ZT9 for both 16S (Student's t test, NA vs. FA: $p = 0.017$; NA vs. FT: $p = 0.01$) and metagenomics (NA vs. FA and NA vs. FT: $p < 0.001$, Figure S1D). These oscillations, observed only in NA mice, suggest diurnal variation in composition and functional potential, consistent with prior studies.[1,7] Interestingly, transcript-level α-diversity did not vary by time (one-way ANOVA, $p = 0.78$, Figures S1C and S1D). These results suggest diet exerts a stronger influence on microbial transcriptional α-diversity than on taxonomic composition or functional potential.

β-diversity analysis showed that both diet and feeding pattern significantly altered microbial composition, based on 16S (PERMANOVA, $p = 0.0012$, Figure 1B). Diet was also the primary driver of functional compositional shifts in both metagenomic and metatranscriptomic profiles (NA vs. FA and NA vs. FT, $p = 0.0015$, Figures 1C and 1D). To assess whether metatranscriptomics is more sensitive to time-dependent effects of TRF than metagenomics, we compared FA and FT β-diversity within each dataset. Metagenomic analysis showed no significant differences ($p = 0.16$, Figure 1C), while metatranscriptomic profiles trended toward significance ($p = 0.073$, Figure 1D), suggesting that metatranscriptomics may better capture TRF-induced functional compositional shifts.

We next evaluated whether collection time influenced β-diversity by comparing light (ZT1–ZT9) and dark (ZT13–ZT21) phases and which omics method best captured these temporal differences. In NA mice, significant diurnal variation was observed across all omics methods (PERMANOVA, 16S: $p = 0.027$, metagenomics: $p = 0.045$, metatranscriptomics: $p = 0.041$, Figure 1E). By contrast, no diurnal differences were detected in FA mice (16S: $p = 0.45$, metagenomics: $p = 0.47$, metatranscriptomics: $p = 0.46$, Figure 1F). TRF did not restore the NA-like diurnal pattern. Instead, FT mice resembled FA mice, showing no significant time-of-day differences across any omics method (16S: $p = 0.79$, metagenomics: $p = 0.74$, metatranscriptomics: $p = 0.71$, Figure 1G). This may reflect differences in feeding status: at ZT13, FT mice are fasted, while NA mice are fed, revealing a shift in feeding relative to diurnal phase. To test this, we reanalyzed FT samples by feeding status (fasted: ZT5–ZT13; fed: ZT17, ZT21, ZT1) across omics methods. Only metatranscriptomics detected significant differences between fasted and fed states ($p = 0.035$, Figure 1G), while 16S and metagenomics showed no such effect ($p = 0.52$ and 0.74, respectively; Figure 1G). These findings indicate that diet strongly shapes the microbial functional landscape and that TRF promotes distinct, feeding-dependent shifts in microbial activity—detectable only through metatranscriptomics.

### Metatranscriptomics captures TRF-driven diurnal differential expression of microbial functions

To evaluate functional differential abundance between conditions, we used ALDEx2—analysis of differential abundance taking sample and scale variation into account, a method designed to identify differentially abundant features in microbiome

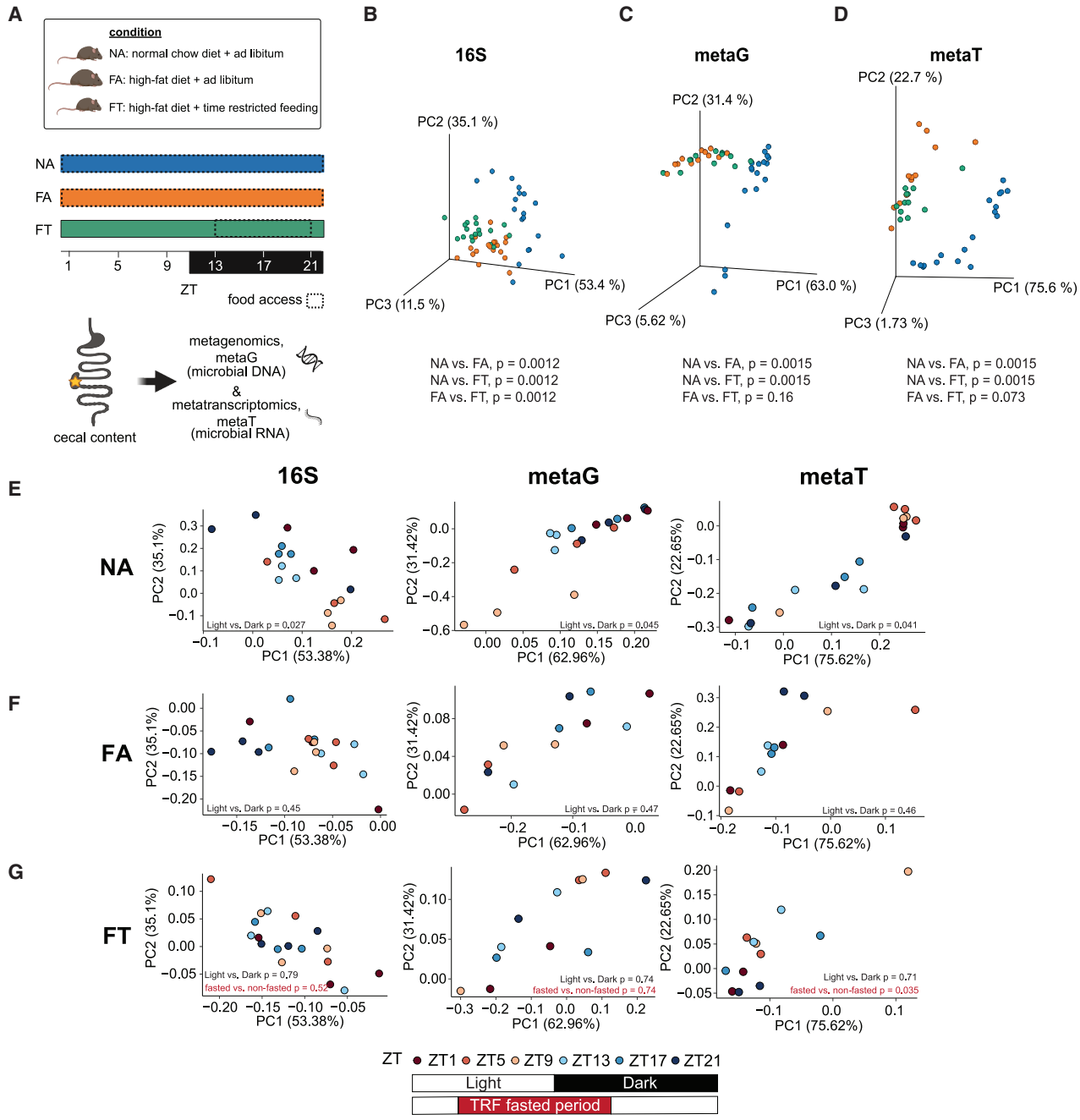


**Figure 1. Metatranscriptomics captures functional dynamics driven by diet and feeding behavior**

(A) Experimental design and sample collection.

(B–D) β-diversity/robust Aitchison based on diet and feeding conditions for 16S composition (B), functional metagenomics (C), and metatranscriptomics (D). $n$ = 12–18 mice/condition; $p$ values from PERMANOVA with $\alpha < 0.05$.

(E–G) β-diversity/robust Aitchison based on ZT separated by (E) NA, (F) FA, and (G) FT and method of analysis (columns). ZT1–9 are considered in the light phase and ZT13–21 in the dark phase. The TRF fasted period is ZT5–13, while its non-fasted/fed period is ZT17, ZT21, and ZT1. $n$ = 6–9 mice/phase/condition; $p$ values from PERMANOVA with $\alpha < 0.05$. metaG, metagenomics; metaT, metatranscriptomics.

See also Figure S1.

and RNA sequencing (RNA-seq) datasets[24,25]—to compare microbial gene (metagenomics) and transcript (metatranscriptomics) profiles independent of time. Diet drove the largest differences across both omics layers, but the extent varied by method. A significantly greater proportion of transcripts were differentially abundant compared with genes between NA and FA ($\chi^2$, $p$ = 0.031) and NA and FT ($p < 0.001$), while the TRF contrast (FA vs. FT) revealed a small yet significant difference

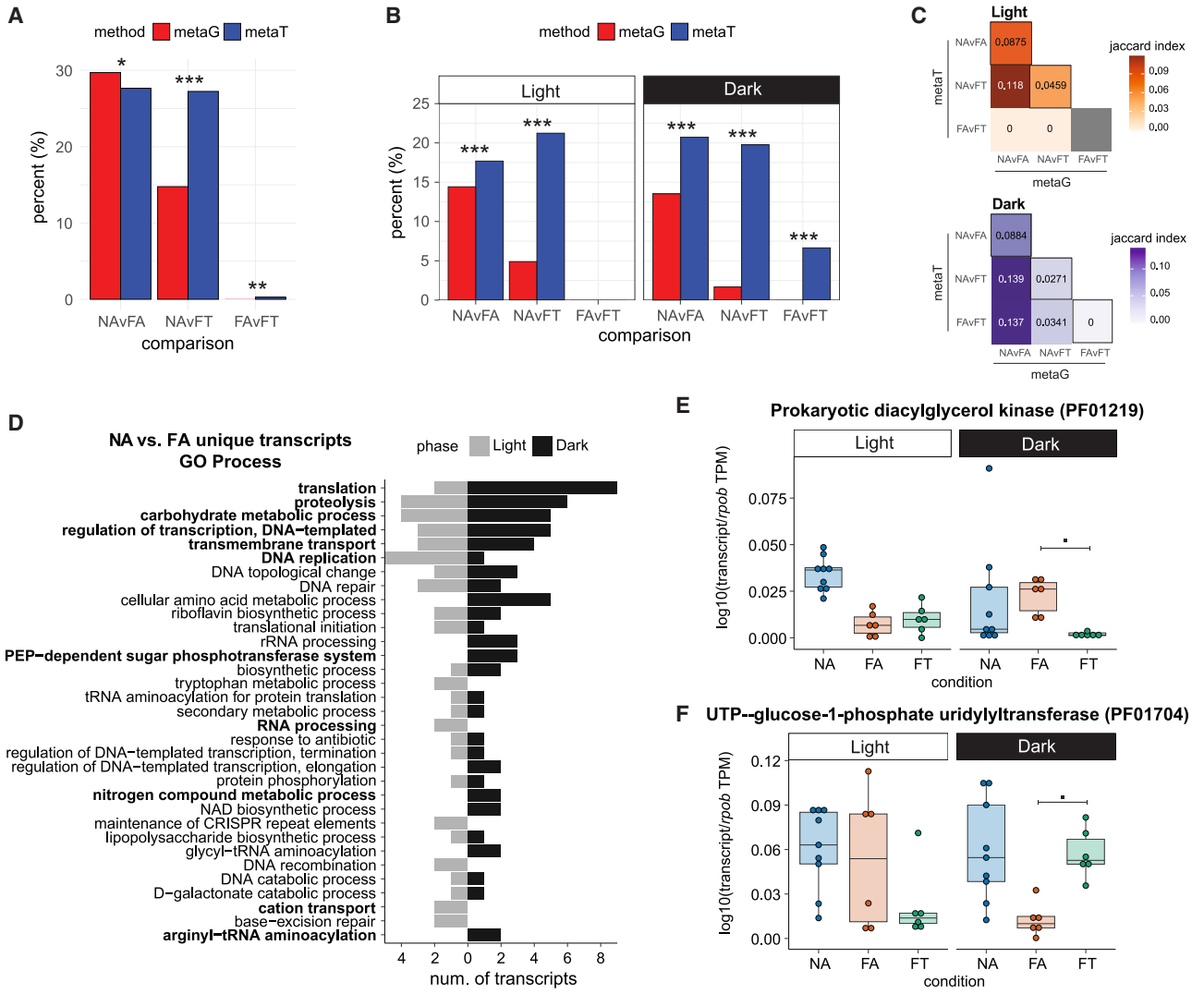


**Figure 2. Metatranscriptomics captures TRF-driven diurnal differential expression of microbial functions**

(A and B) Percent of transcriptional and gene results determined using ALDEx2 and $\alpha < 0.1$ that are differentially expressed between conditions in the metagenomics and metatranscriptomics when (A) not accounting for time ($n$ = 12–18 mice/condition) and (B) stratifying by light and dark phase ($n$ = 6–9 mice/phase/condition). ***$p < 0.001$, **$p < 0.01$, *$p < 0.05$ using $\chi^2$ test.

(C) Jaccard distance showing the similarity of the differentially expressed transcripts and abundant genes between conditions in the metatranscriptomics and metagenomics for the light (left) or dark (right) phase.

(D) Summary of GO processes represented in the metatranscriptomics data that were differentially expressed between NA and FA in the light and dark phase. Bold GO processes are shared with those differentially expressed between NA and FT.

(E and F) Transcripts of interest that were differentially expressed between FA and FT in the dark phase that are more highly expressed under either (E) FA or (F) FT ($n$ = 6–9 mice/phase/condition; ALDEx2. $p < 0.1$). metaG, metagenomics; metaT, metatranscriptomics.

See also Figure S2 and Tables S1 and S2.

($p = 0.004$), with 0.28% of transcripts differentially expressed and no gene-level differences (Figure 2A; Table S1). These results confirm diet as the primary driver of microbial functional change and suggest that metatranscriptomics detects finer TRF-related shifts not captured by metagenomics.

Because time of sample collection can affect microbiome results,[26] we stratified samples by light (ZT1–ZT9) and dark (ZT13–ZT21) phases to assess whether metatranscriptomics more effectively captures TRF-driven changes. This analysis revealed a diurnal, TRF-specific transcriptional response. In the dark phase—but not the light—significantly more transcripts were differentially expressed between FA and FT in the metatranscriptomics, an effect not observed in the metagenomics ($\chi^2$, $p < 0.001$; Figure 2B; Table S2). In fact, there were no gene-level TRF contrast differences in either the light or dark phase (Figure 2B; Table S2). Echoing our time-independent analysis, metatranscriptomics revealed more significant differences between NA and either HFD condition (FA or FT) than metagenomics across both light and dark phases ($p < 0.001$, Figure 2B). These results were consistent even after rarefying the metatranscriptomic

data to match the metagenomic sequencing depth (Figure S2A). Finally, Jaccard distance analysis of differentially expressed features revealed minimal overlap between genes and transcripts across conditions and diurnal phases (Figure 2C). These observations indicate that microbial gene content does not reliably reflect transcriptional activity.

Since metatranscriptomics captured diurnal TRF-specific expression changes, we next examined transcripts differentially expressed across conditions (NA, FA, and FT). Jaccard distance analysis of pairwise comparisons in both light and dark phases revealed minimal overlap in differentially expressed transcripts between phases (Figure S2B). Despite this, Gene Ontology (GO) enrichment revealed similar biological processes affected in both phases. In particular, the diet comparison between NA and FA showed transcriptional changes in translation, proteolysis, and carbohydrate metabolism across both phases (Figure 2D), with similar patterns observed in the NA vs. FT comparison (Figure S2C). These results suggest that diet induces phase-independent transcriptional shifts in core microbial functions.

We summarized GO processes for the FA vs. FT comparison across light and dark phases but observed no clear patterns, likely due to sparse annotation, with most GO terms linked to a single transcript (Figure S2D). However, focused analysis of transcripts differentially expressed between FA and FT only in the dark phase revealed enrichment in genes related to lipid and carbohydrate metabolism. For example, diacylglycerol kinase and enoyl-acyl carrier protein (ACP) reductase—enzymes in lipid signaling and fatty acid synthesis[27,28]—were more highly expressed under FA than FT (Figures 2E and S2E). By contrast, uridine triphosphate (UTP)–glucose-1-phosphate uridylyltransferase and chemotaxis receptor (CheR) methyltransferase—involved in carbohydrate metabolism and chemotaxis[29,30]—were more expressed under FT than FA (Figures 2F and S2F). These findings suggest TRF modulates microbial lipid and carbohydrate gene expression in a time-dependent manner, specifically during the dark phase.

## Metatranscriptomics captures functional cyclical fluctuations driven by diet and feeding behavior

Microbial communities are dynamic, exhibiting diurnal fluctuations over 24h,[1,26] but whether microbial transcripts follow similar rhythmic patterns remains unclear. To investigate this, we compared cycling behavior in microbial genes (metagenomics) and transcripts (metatranscriptomics). In NA mice, ~8% of both genes and transcripts showed diurnal oscillation. This rhythmicity was significantly reduced under FA in both omics methods ($\chi^2$, metagenomics: $p < 0.001$; metatranscriptomics: $p < 0.001$, Figure 3A; Table S3), consistent with prior reports of HFD-induced loss of microbial cycling.[1,2] In metagenomics, the number of cycling genes in FT was comparable to FA ($p = 0.83$). By contrast, metatranscriptomics revealed that TRF preserves transcript cycling lost under FA ($p < 0.001$), reaching levels comparable to or slightly higher than NA (9%). Despite the larger number of transcripts (over 7,000 vs. ~3,500 genes), rarefaction of the metatranscriptomic data to match metagenomic depth still showed significantly more cycling transcripts in FT than FA ($p < 0.001$, Figure S3A), indicating that this effect was not due to sequencing depth. Thus, metatranscriptomics—but not metagenomics—captures the dynamic nature of the luminal environment induced by TRF.

There was minimal overlap in cycling features across conditions (Figure 3B) or between omics types (Figure 3C), even after rarefaction (Figures S3B and S3C), suggesting distinct rhythmic profiles by condition and method. Importantly, cycling detected at the DNA level does not imply rhythmic transcriptional activity.

Given that metatranscriptomics more accurately reflects functional cycling, we focused further analyses on this method type. While TRF restored transcriptional cycling, only 10% of FT cycling transcripts overlapped with those from either NA or FA (Figure 3B), indicating that TRF induces a distinct rhythmic profile. To determine whether shared cycling transcripts maintained consistent timing, we analyzed phase distribution. Transcripts cycling in both FA and FT (but not NA, Figure 3D) peaked at ZT17 (dark) under FA and ZT9 (light) under FT, indicating a TRF-induced phase shift (Figure 3E). Transcripts shared between NA and FT peaked at ZT9 with a secondary peak at ZT17 (Figure 3F). Many of these transcripts that cycled in at least two conditions were related to lipid and glucose metabolism (Figures S3D and S3E). These findings suggest that TRF can preserve the normal cycling patterns disrupted by HFD, which may underlie its ability to prevent the adverse physiological effects associated with DIO.

We also examined the unique cycling metatranscriptional profiles of each condition. In NA mice, most uniquely cycling transcripts were associated with translation and regulation of transcription and carbohydrate metabolic processes (Figure 3G). Notably, transcripts for acyl-coenzyme A (CoA) dehydrogenase, which catalyzes the first step in fatty acid β-oxidation, and glycerol-3-phosphate (G3P) acyltransferase, a rate-limiting enzyme in *de novo* glycerolipid synthesis,[31,32] both exhibited rhythmic expression (Figure 3H). Acyl-CoA dehydrogenase expression showed a trough, while G3P acyltransferase expression peaked during the light (inactive) phase. In FT mice, uniquely cycling transcripts were enriched in proteolysis and carbohydrate metabolic processes (Figure 3I) but also included lipid metabolism genes. Enoyl-ACP reductase, involved in fatty acid elongation, and diacylglycerol kinase, which converts diacylglycerol to phosphatidic acid,[28,33] cycled exclusively under FT (Figure 3J), with both showing reduced expression during the dark phase—suggesting that TRF may suppress microbial fatty acid synthesis in the gut lumen at this time period. FA mice exhibited very few cycling transcripts (Figure S3F), limiting interpretation. However, among those detected were genes related to antibiotic resistance (*erythromycin esterase*) and CRISPR maintenance (*Cas5*) (Figure S3G). Together, these findings suggest that TRF restores cycling of bacterial glucose and lipid metabolism transcripts, with peak expression more prominent during the light phase.

## The *bsh* of *D. newyorkensis* exhibits time-dependent differential expression

Thus far, we have established that metatranscriptomics effectively captures time-dependent microbial responses to diet and feeding pattern. We also described how TRF influences the differential abundance and cycling of transcripts related to bacterial lipid and glucose metabolism. One bacterial enzyme we were interested in exploring further using metatranscriptomics was BSH, due to its role in BA modification and its relevance to host health. BSH deconjugates BAs, reducing their polarity

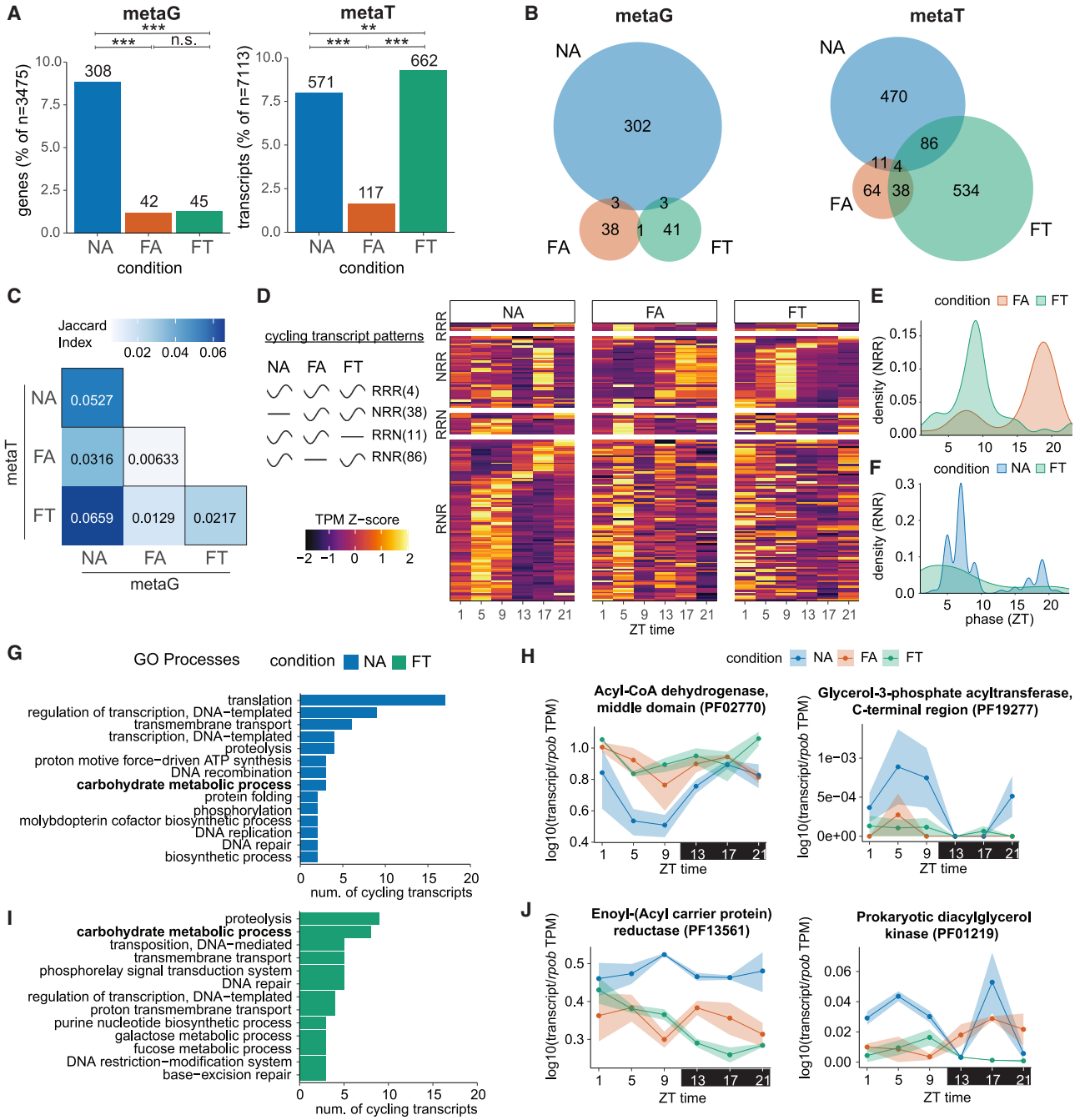


**Figure 3. Metatranscriptomics captures functional cyclical fluctuations driven by diet and feeding behavior**

(A) Summary of cycling results determined using MetaCycle ($n$ = 12–18 mice/condition; $p < 0.05$) in the metagenomic and metatranscriptomic data. $^{**}p < 0.01$, $^{***}p < 0.001$; n.s., not significant using $\chi^2$ test.

(B) Venn diagram showing the overlap of functional results among the diet and feeding conditions for the metagenomics and metatranscriptomics.

(C) Jaccard distance showing the similarity among the cycling results in the metatranscriptomics and metagenomics for each condition.

(D) Heatmap of transcript abundance at each ZT for the functional results that were cycling in at least two conditions.

(E and F) Density plots illustrating cycling phases of transcripts shared between (E) FA and FT and (F) NA and FT.

(G) Top GO processes represented in the cycling metatranscriptomics results unique to the NA condition.

(H) Representative fatty acid metabolism transcripts that cycled just in NA.

(I) Top GO processes represented in the cycling metatranscriptomics results unique to the FT condition.

(J) Representative fatty acid metabolism transcripts that cycled just in FT. ZT1–12 indicates the light phase (white), and ZT12–23 the dark phase (black). N, not rhythmic; R, rhythmic; metaG, metagenomics; metaT, metatranscriptomics.

See also Figure S3 and Table S3.

and reabsorption and altering their activity at various BA and sterol receptors. More recent studies also show that BSH has amidation activity, leading to the production of a wide array of previously uncharacterized conjugated BAs.[34]

Our previous work shows that NA mice have a higher ratio of deconjugated to conjugated BAs during the light but not the dark phase. This pattern is disrupted under FA but restored in FT (Figure S4A),[1,3] supporting the potential role of BAs acting as feeding or circadian entraining agents for peripheral, metabolically important organs (e.g., liver, intestines, etc.).[35–37] We therefore hypothesized that *bsh* expression would follow a similar pattern—elevated in the light phase under NA and FT and disrupted under FA (Figure 4A). However, differential expression and cycling analyses did not identify *bsh* as a TRF-responsive diurnal transcript. Instead, *bsh* expression was diet-dependent (NA vs. FA and NA vs. FT, ALDEx2 $p < 0.001$) and showed no significant TRF-driven differences (FA vs. FT, $p = 0.23$) or evidence of diurnal cycling (Tables S1, S2, and S3).

To investigate further, we quantified total *bsh* expression normalized to RNA polymerase B (*rpoB*, a housekeeping transcript) across the entire microbiome, not separating by species. NA mice had significantly higher *bsh* expression than both FA and FT, regardless of phase (Mann-Whitney U test, light: $p = 0.0012$, dark: $p < 0.001$), with no TRF-specific differences (FA vs. FT, light: $p = 0.59$, dark: $p = 0.065$; Figure 4B). We verified these findings using a curated BSH protein database to search and quantify the metatranscriptomics data. This targeted analysis also showed higher *bsh* expression in NA compared with FA and FT (top/bottom 10% transcript ratio, light: $p < 0.001$, dark: $p = 0.0012$), with no difference between FA and FT in either phase (light: $p = 0.59$, dark: $p = 0.18$, Figure 4C). These results suggest that overall *bsh* expression is not subject to TRF-driven temporal variation, though coverage limitations in the database remain possible.

Given the functional diversity of BSH enzymes in the microbiome[39,40] and the observed variation in *bsh* expression across known taxa in a species-level summary (Figure S4B), we hypothesized that these species-specific differences may be masked in bulk expression data. To test this, we used BIRDMAn (Bayesian inferential regression for differential microbiome analysis), a Bayesian differential abundance framework,[38] to analyze *bsh* expression by species across conditions and diurnal phases. In the NA vs. FA comparison, *bsh* expression varied widely across taxa, with some transcripts exhibiting potential diurnal differences (Figures S4C and S4D; Table S4). Interestingly, *Lachnospiraceae CAG-95*, *Eubacterium_J plexicaudatum*, and *Lachnospiraceae 14-2* (highlighted in blue) had credibly (the high-density interval [hdi] excluded 0) higher *bsh* expression in NA during both phases. By contrast, *Lachnospiraceae CAG-317* and *Lactobacillus gasseri* (highlighted in orange) were enriched under FA. While *CAG-317 bsh* was consistently enriched in both phases, *L. gasseri bsh* (LgBSH) was enriched only in the dark phase but exhibited a larger overall effect size (Figures S4C and S4D). These results demonstrate species-level variation in diet-associated *bsh* expression, regardless of diurnal phase.

In the FA vs. FT comparison, species-level *bsh* expression also showed high variability (Table S4). *Lachnospiraceae 14-2*, previously enriched in NA relative to FA, was similarly enriched in FT during the dark phase (Figure 4D). However, only one *bsh*—from *D. newyorkensis*—showed credible TRF-specific enrichment: it was enriched under FA in the dark phase and showed borderline enrichment under FT in the light phase. This pattern corroborates our hypothesis, with higher expression in the light phase and reduced expression in the dark phase under TRF.

We also repeated this analysis using a targeted search for *bsh* transcripts to validate our untargeted findings. The results were consistent: two *D. newyorkensis bsh* transcripts (protein IDs A0A1U7NP31 and A0A1U7NKD7) showed credible enrichment under FA in the dark phase and borderline enrichment under FT in the light phase (highlighted in green, Figure 4E; Table S4). Additional *bsh* transcripts from *Bacteroides uniformis* followed a similar diurnal enrichment pattern but were not detected in the untargeted analysis. Finally, when we performed this analysis using metagenomics, no *bsh* gene showed significant diurnal or TRF-specific abundance differences (Figures S4E–S4G). Together, these results indicate that *D. newyorkensis bsh* exhibits a diurnal expression pattern consistently captured by metatranscriptomics but not by metagenomics.

## TRF identified BSHs have an increased capacity for amidation

Through both targeted and untargeted searches of *bsh* transcripts, we identified species-level variation in *bsh* expression, with some microbes exhibiting higher expression under specific conditions. Among these, two unique *bsh* transcripts from *D. newyorkensis*—exclusive to TRF and showing time-dependent expression differences—were of particular interest. To investigate their potential functional contribution to TRF's physiological effects, we engineered these and other selected *bsh* genes into a previously characterized native *E. coli* chassis, EcAZ, which expresses genes under a constitutive promoter.[10,41] We selected this chassis for its ability to stably colonize the gut after a single gavage without antibiotic pretreatment[42] and to introduce new functions and metabolites into the gut lumen without altering microbiome composition—making it an ideal tool for studying specific microbial functions.[10,41]

We selected seven *bsh* candidates for engineering: (1) *D. newyorkensis* A0A1U7NKD7 (DnBSH1), (2) *D. newyorkensis* A0A1U7NP31 (DnBSH2), (3) *Lactobacillus gasseri* (LgBSH), (4) *Eubacterium plexicaudatum* (EpBSH), (5) *Lachnospiraceae CAG-95* (LCAG95BSH), (6) *Lachnospiraceae 14-2*, and (7) *Bacteroides uniformis* A0A3E5F5J9. Selection was based on TRF-driven diurnal expression (DnBSHs, *B. uniformis*), enrichment under FA (*L. gasseri*), and consistent expression under NA (*E. plexicaudatum*, *Lachnospiraceae CAG-95*) (Figures 4D, 4E, S4C, and S4D). Five of seven *bsh* genes were successfully engineered (Figure 5A), and the *B. uniformis* and *Lachnospiraceae 14–2 bsh* constructs could not be maintained due to mutations likely affecting the fitness of the *E. coli* chassis.

To evaluate deconjugation activity, we cultured each BSH-expressing engineered native bacteria (ENB) in rich media supplemented with one of ten glycine- or taurine-conjugated BAs and performed untargeted liquid chromatography tandem mass spectrometry (LC-MS/MS) at 0 and 48 h (Figure 5B). Significant differences in the abundance of known or predicted BA were observed between strains and supplemented BAs over time (Student's t test, $p < 0.05$, Figure S5A; Table S5). Annotations were confirmed by MS/MS and retention time matching to

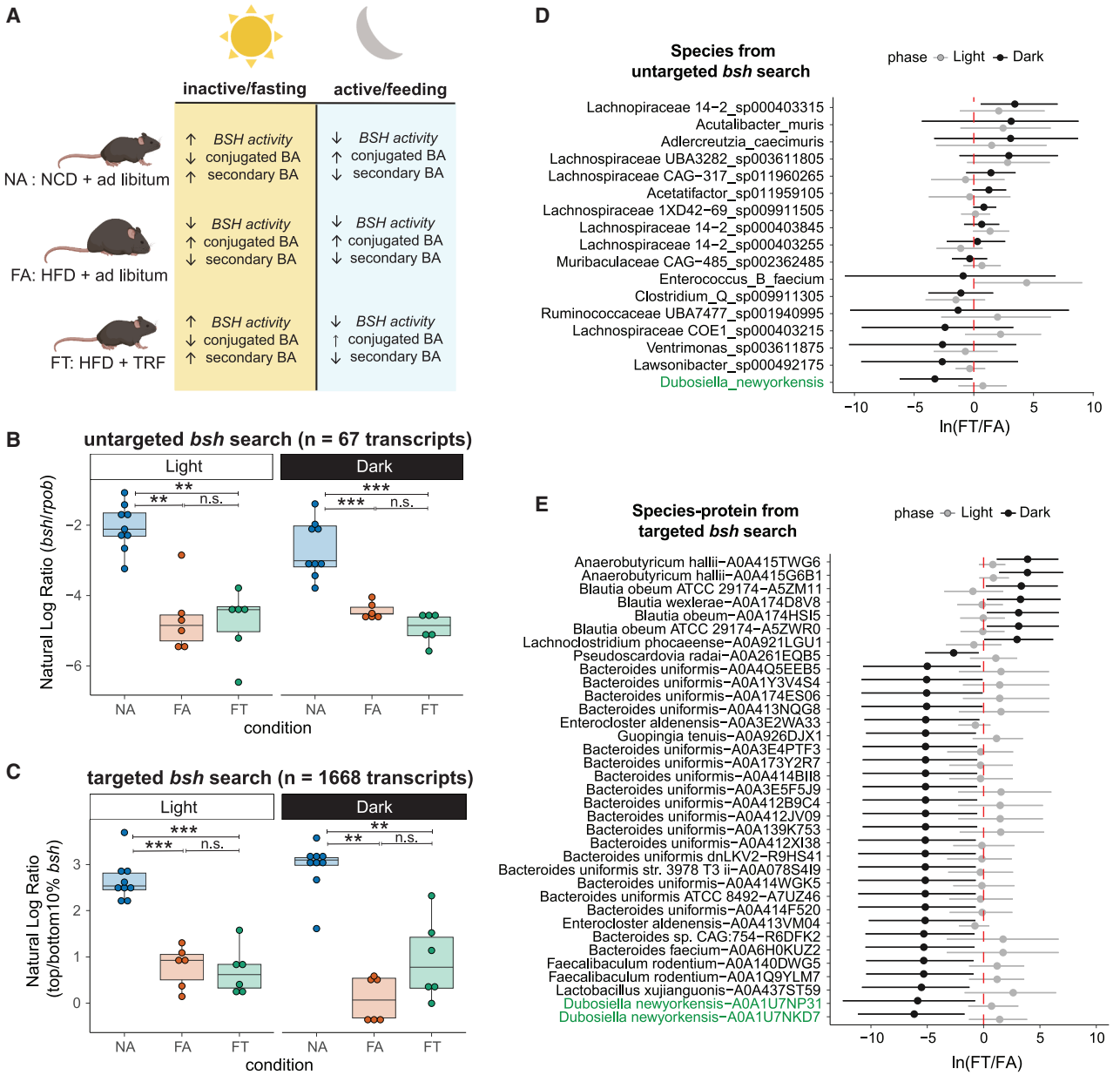


**Figure 4. The *bile salt hydrolase* of *Dubosiella newyorkensis* exhibits time-dependent differential expression**

(A) Schematic describing the hypothesized BSH activity based on changes in conjugated and secondary BAs in the diet and feeding conditions stratified by phase.

(B) Natural log ratio of *bsh* to *rpob* transcripts separated by condition and phase from the untargeted search for *bsh* in the WoL2 database ($n$ = 6–9 mice/phase/condition; pairwise Mann-Whitney U test, ***$p$ < 0.001, **$p$ < 0.01, *$p$ < 0.05; n.s., not significant).

(C) Natural log ratio of the top and bottom 10% of *bsh* transcripts separated by condition and phase from the targeted *bsh* search using a curated database of BSH proteins ($n$ = 6–9 mice/phase/condition; pairwise Mann-Whitney U test, ***$p$ < 0.001, **$p$ < 0.01, *$p$ < 0.05; n.s., not significant).

(D and E) Ratio of *bsh* expression between FA and FT in either the light or dark phase: (D) untargeted *bsh* search of species with *bsh* arranged by the effect size of credible results in the light phase and (E) targeted *bsh* search species-protein matches ordered by the effect size of credible results in the dark phase ($n$ = 6–9 mice/phase/condition; BIRDMAn,[38] hdi range < 10, credible if the hdi does not cross 0). hdi, high-density interval.

See also Figure S4 and Table S4.

synthetic standards (Figure S5B). Deconjugation capacity, inferred from reduced levels of supplemented BAs from baseline, varied by ENB strain and culture (Student's t test, $p$ < 0.05, Figure 5C). For example, EcAZ-1$^{DnBSH1}$ reduced both glycine- and taurine-conjugated BAs, whereas EcAZ-2$^{BSH*}$ (expressing a well-described *Lactobacillus salivarius bsh*)[10,11,43] reduced only taurine-conjugated BAs (Figure 5C). Despite both possessing a taurine-preferring GTG motif (Figure 5D),[44] EcAZ-1$^{DnBSH1}$

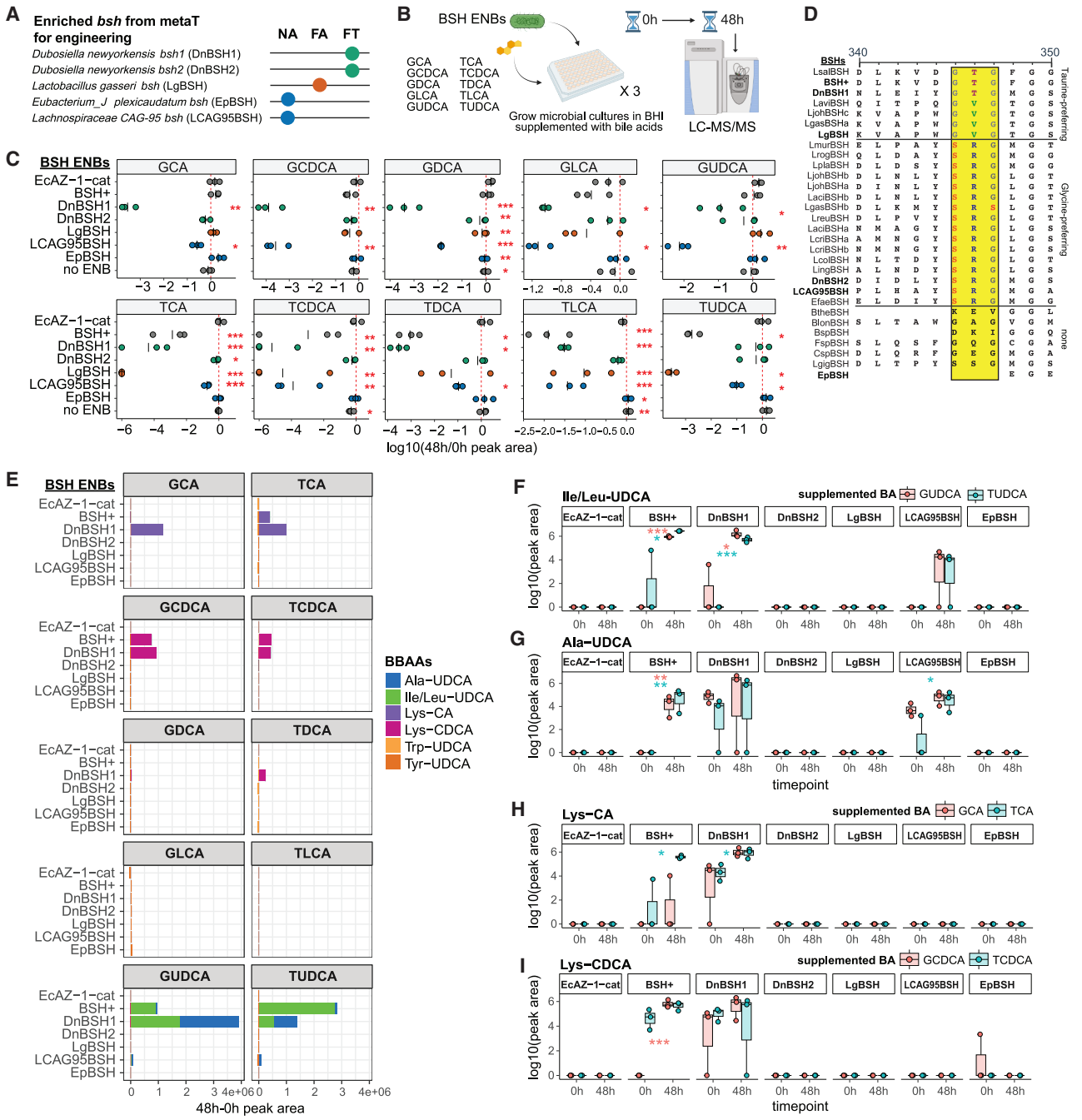


**Figure 5. TRF identified BSHs have an increased capacity for amidation**

(A) *bsh* chosen and successfully engineered based on the diet and feeding conditions its expression was most enriched in.

(B) Design of the culture experiment performed on the various BSH ENBs.

(C) Change from baseline of the BA supplemented into the cultures, a measurement of the deconjugative activity of BSH, for each of the BSH ENBs ($n = 3$ cultures/time point/BA supplement/BSH ENB; Student's t test, $^{***}p < 0.001$, $^{**}p < 0.01$, $^{*}p < 0.05$).

(D) Protein sequence alignment using CLUSTAL Omega, highlighting the selectivity loop region containing motifs associated with taurine or glycine preference.

(E) Difference in the normalized abundance of amidated BAs between 0 and 48 h in the cultures of BSH ENBs, faceted by the different BAs supplemented in the cultures.

(F–I) BBAAs with significant normalized abundance differences between 0 and 48h for EcAZ-2$^{BSH+}$ and EcAZ-1$^{DnBSH1}$ in the (F and G) GUDCA and TUDCA and (H and I) other BA-supplemented cultures ($n = 3$ cultures/time point/BA supplement/BSH ENB; Student's t test, $^{***}p < 0.001$, $^{**}p < 0.01$, $^{*}p < 0.05$). BSH+ = EcAZ-2$^{BSH+}$; DnBSH1 = EcAZ-1$^{DnBSH1}$; DnBSH2 = EcAZ-1$^{DnBSH2}$; LgBSH = EcAZ-1$^{LgBSH}$; LCAG95BSH = EcAZ-1$^{LCAG95BSH}$; EpBSH = EcAZ-1$^{EpBSH}$. GCA, glycocholic acid; GCDCA, glycochenodeoxycholic acid; GDCA, glycodeoxycholic acid; GLCA, glycolithocholic acid; GUDCA, glycoursodeoxycholic acid; TCA, taurocholic acid; TCDCA, taurochenodeoxycholic acid; TDCA, taurodeoxycholic acid; TLCA, taurolithocholic acid; TUDCA, tauroursodeoxycholic acid. BlonBSH,

*(legend continued on next page)*

exhibited broader substrate promiscuity compared with EcAZ-$2^{BSH^*}$. Similarly, EcAZ-$1^{LCAG95BSH}$ deconjugated both taurine and glycine conjugates despite having a glycine-selective SRG motif. These findings indicate that the BSH ENBs differ in substrate specificity and that factors beyond the selectivity loop motif likely contribute to their deconjugation activity.

BSHs can catalyze amidation reactions,[34,45] prompting our investigation into amidation activity across BSH ENB cultures. Several bacterial bile acid amidates (BBAAs) differed significantly between 0 and 48 h (Figure S5A). Using retention time matching, we validated four of six BBAAs detected in culture (Figures 5E, S5C, and S5D), and Trp- and Tyr-ursodeoxycholic acid (UDCA) were excluded as background culture components potentially modulated by BSHs. After normalizing to a no-ENB control to assess BBAA abundance change over time—our proxy for measuring amidation activity—we observed that EcAZ-$2^{BSH^*}$ and EcAZ-$1^{DnBSH1}$ exhibited similar amidation profiles (Figure 5E). For instance, isoleucine/leucine-conjugated UDCA (Ile/Leu-UDCA) increased significantly in both strains when cultured with tauroursodeoxycholic acid (TUDCA) (Student's t test, EcAZ-$2^{BSH+}$: $p = 0.040$, EcAZ-$1^{DnBSH1}$: $p < 0.001$) or glycoursodeoxycholic acid (GUDCA) (EcAZ-$2^{BSH+}$: $p < 0.001$, EcAZ-$1^{DnBSH1}$: $p = 0.015$, Figure 5F). In addition, alanine-conjugated UDCA (Ala-UDCA) increased in the EcAZ-$2^{BSH^*}$ cultures (TUDCA: $p = 0.002$, GUDCA: $p = 0.002$) but not in EcAZ-$1^{DnBSH1}$ (TUDCA: $p = 0.65$, GUDCA: $p = 0.83$), likely due to high baseline levels at t = 0 (Figure 5G). Both strains produced lysine-conjugated cholic acid (Lys-CA) in taurocholic acid (TCA) cultures (EcAZ-$2^{BSH+}$: $p = 0.025$, EcAZ-$1^{DnBSH1}$: 0.026, Figure 5H), while lysine-conjugated chenodeoxycholic acid (Lys-CDCA) increased only in EcAZ-$2^{BSH^*}$ in the glycochenodeoxycholic acid (GCDCA) culture ($p < 0.001$) and not in EcAZ-$1^{DnBSH1}$, again likely due to high starting abundance (Figure 5I). Given sampling lag, the patterns observed for Ala-UDCA and Lys-CDCA with EcAZ-$1^{DnBSH1}$ suggest this strain may produce BBAAs more rapidly than EcAZ-$2^{BSH}$. Aside from Ala-UDCA—which also increased in EcAZ-$1^{LCAG95BSH}$ with TUDCA ($p = 0.046$)—these BBAAs were unique to EcAZ-$2^{BSH+}$ and EcAZ-$1^{DnBSH1}$. Interestingly, despite sharing the most closely related BSH protein sequences (Figures S5E and S5F), EcAZ-$1^{DnBSH1}$ and EcAZ-$1^{DnBSH2}$ differed in both deconjugation and amidation activity, highlighting the functional specificity of individual BSHs. Overall, EcAZ-$2^{BSH^*}$ and EcAZ-$1^{DnBSH1}$ exhibit similar deconjugation and amidation capacities, which may underlie comparable phenotypic effects *in vivo*.

## Engineered *E. coli* expressing DnBSH1 has a more pronounced phenotypic effect than other BSHs

BA quantification revealed that EcAZ-$2^{BSH+}$ and EcAZ-$1^{DnBSH1}$ exhibit similar amidation activity. We previously showed that EcAZ-$2^{BSH+}$ can improve insulin sensitivity and glucose tolerance in fully conventional mice when tested 12 weeks after a single gavage.[10] To investigate whether EcAZ-$1^{DnBSH1}$ can produce similar metabolic effects to EcAZ-$2^{BSH+}$, we introduced it, along with EcAZ-$1^{LgBSH}$ (from FA mice, no amidation activity) and EcAZ-2 (empty chassis), into 8-week-old fully conventional C57BL/6 male mice on a NCD and assessed metabolic outcomes at a shorter time interval, 6 weeks after a single gavage (Figure 6A).

All BSH ENBs successfully colonized the host (Figure 6B), with no significant differences in colonization levels ($n = 10$/group, pairwise Student's t test, $\alpha < 0.05$). However, qualitative differences in taurodeoxycholic acid (TDCA) deconjugation emerged after fecal isolation: EcAZ-$1^{DnBSH1}$ showed less TDCA deconjugation than EcAZ-$2^{BSH^*}$ and EcAZ-$1^{LgBSH}$, indicated by fewer deoxycholic acid (DCA) precipitates (Figure 6C). Food intake and body weight also did not differ across groups ($n = 10$ mice/group; pairwise Student's t test, $\alpha < 0.05$, Figures 6D and 6E). These outcomes are consistent with earlier findings for EcAZ-2 $^{BSH+}$.[10]

EcAZ-$2^{BSH^*}$ significantly reduced postprandial blood glucose compared with EcAZ-2 (Student's t test, $p = 0.011$), consistent with prior findings. EcAZ-$1^{DnBSH1}$ also lowered postprandial glucose ($p = 0.041$), whereas EcAZ-$1^{LgBSH}$ had no effect (Figure 6F). Although EcAZ-$2^{BSH^*}$ did not reduce postprandial insulin at this 6-week time point ($p = 0.22$), our previous studies showed robust reduction at 12 weeks. By contrast, EcAZ-$1^{DnBSH1}$ significantly lowered insulin at 6 weeks levels ($p = 0.02$), while EcAZ-$1^{LgBSH}$ again showed no effect (Figure 6G). Fasting glucose was unaffected by EcAZ-$2^{BSH^*}$ ($p = 0.316$) but decreased in mice engrafted with EcAZ-$1^{DnBSH1}$ ($p = 0.028$) and EcAZ-$1^{LgBSH}$ (Student's t test, $p = 0.0044$; Figure S6A). These findings suggest that EcAZ-$1^{DnBSH1}$ may improve insulin sensitivity and glucose homeostasis more effectively than EcAZ-$2^{BSH^*}$.

Body composition analysis revealed no change in fat or lean mass with EcAZ-$2^{BSH^*}$ or EcAZ-$1^{LgBSH}$ (Figures 6H and 6I). By contrast, EcAZ-$1^{DnBSH1}$ significantly decreased fat mass ($p = 0.0075$) and increased lean mass ($p = 0.033$) compared with EcAZ-2. These results suggest that EcAZ-$1^{DnBSH1}$ influences lipid deposition more effectively than EcAZ-$2^{BSH^*}$ and may offer greater overall metabolic benefits.

To investigate *in vivo* BA modification by the BSH ENBs, we performed untargeted LC-MS/MS on fecal samples collected at ZT3 and ZT15 and assessed BA profiles by phase. These time points were selected because, although the *bsh* transgenes were driven by constitutive promoters, circadian variation from the host or microbiome could still influence BA dynamics. The BSH ENBs altered the fecal BA pool (Figure S6B; Table S6), and one BBAA, Ser-CDCA, was significantly enriched in EcAZ-$1^{DnBSH1}$ vs. EcAZ-2—specifically in the light phase (Tukey's

*Bifidobacterium longum* BSH; BspBSH, Bacteroidales sp. BSH; BtheBSH, *Bacteroides thetaiotaomicron* BSH; CspBSH, Clostridiales sp. BSH; EfaeBSH, *Enterococus faecalis* BSH; FspBSH, Faecalibacterium sp. BSH; LaciBSHa, *Lactobacillus acidophilus* BSHa; LaciBSHb, *Lactobacillus acidophilus* BSHb; LaviBSH, *Ligilactobacillus aviarius* BSH; LcolBSH, *Limosilactobacillus coleomonis* BSH; LcriBSHa, *Lactobacillus crispatus* BSHa; LcriBSHb, *Lactobacillus crispatus* BSHb; LgasBSHa, *Lactobacillus gasseri* BSHa; LgasBSHb, *Lactobacillus gasseri* BSHb; LgigBSH, *Lactobacillus gigeriorum* BSH; LingBSH, *Limosilactobacillus ingluveiei* BSH; LjohBSHa, *Lactobacillus johnsonii* BSHa; LjohBSHb, *Lactobacillus johnsonii* BSHb; LjohBSHc, *Lactobacillus johnsonii* BSHc; LmurBSH, *Ligilactobacillus murinus* BSH; LplaBSH, *Lactiplantibacillus plantarum* BSH; LreuBSH, *Limosilactobacillus reuteri*; LrogBSH, *Lactobacillus rogoseae* BSH; LsalBSH, *Ligilactobacillus Salivarius* BSH. Ile/Leu-UDCA, isoleucine/leucine-conjugated ursodeoxycholic acid; Ala-UDCA, alanine-conjugated ursodeoxycholic acid; Lys-CA, lysine-conjugated cholic acid; Lys-CDCA, lysine-conjugated chenodeoxycholic acid.
See also Figure S5 and Table S5.

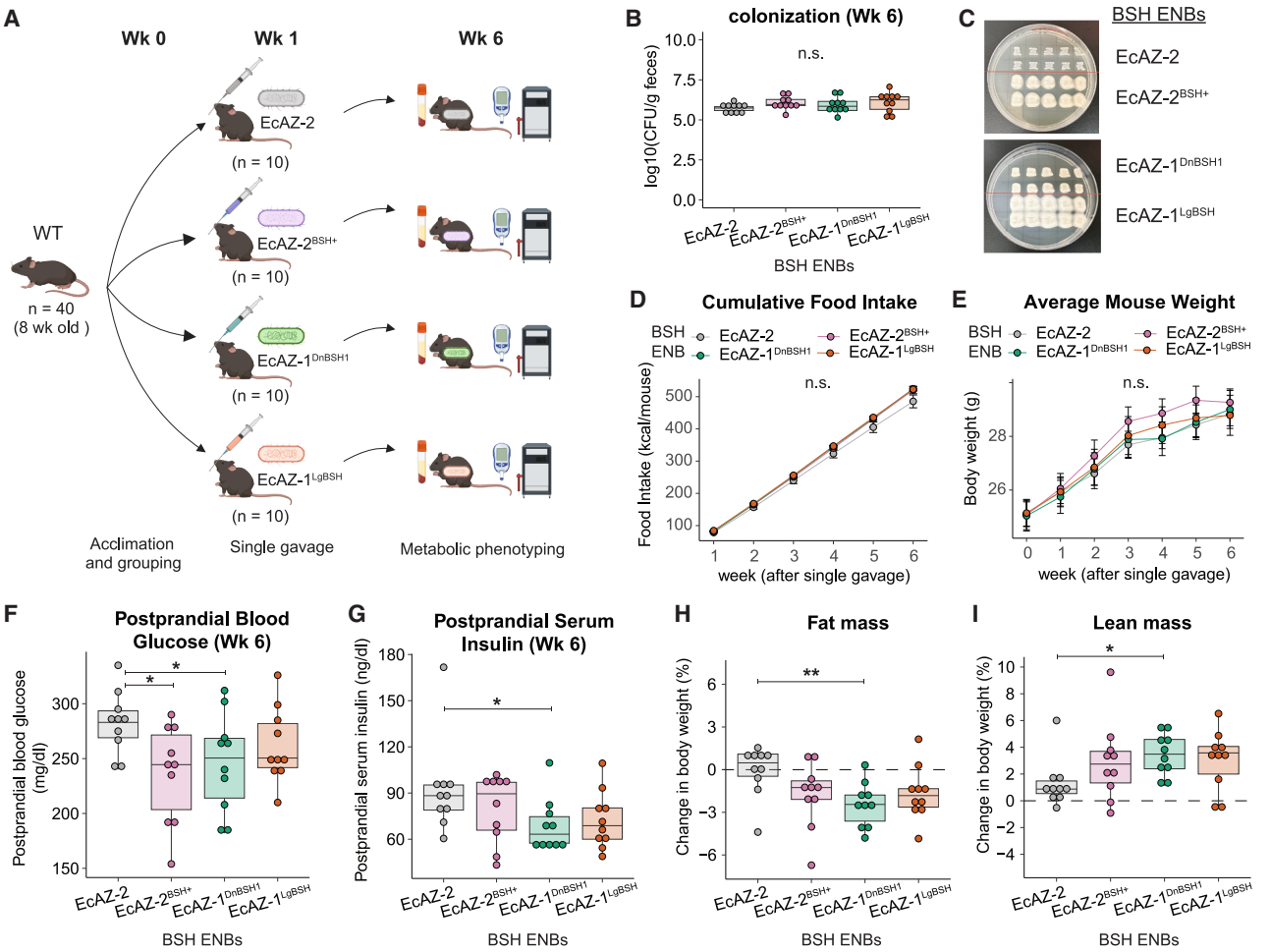


**Figure 6. Engineered *E. coli* expressing *D. newyorkensis bsh1* has a more pronounced phenotypic effect than other BSHs**

(A) Experimental design and sample collection protocol.

(B) Colonization of the BSH ENBs 6 weeks post single gavage ($n$ = 10 mice/group; pairwise Student's t test; n.s., not significant at $\alpha < 0.05$).

(C) Plating of fecal samples from mice gavaged with the BSH ENBs on LB containing TDCA plates. White precipitate around colonies indicates BSH is deconjugating TDCA to DCA, qualitatively indicating enzyme functionality.

(D and E) (D) Average cumulative food intake and (E) body weight of mice after single gavage ($n$ = 10 mice/group; pairwise Student's t test; n.s., not significant at $\alpha < 0.05$).

(F and G) Postprandial (F) blood glucose and (G) serum insulin concentrations of mice 6 weeks post single gavage ($n$ = 10 mice/group; pairwise Student's t test, $^*p < 0.05$).

(H and I) Percent change in (H) fat and (I) lean mass from week 0 to 6 ($n$ = 10 mice/group; pairwise Student's t test, $^{**}p < 0.01$, $^*p < 0.05$).

See also Figure S6 and Table S6.

LSD, $p$ = 0.017). This suggests that EcAZ-1$^{DnBSH1}$ may confer metabolic benefits through either direct or indirect phase-dependent modification of the luminal BA pool.

## DISCUSSION

This study highlights the unique value of metatranscriptomics in capturing time-dependent microbial changes that remain undetectable with metagenomics. Unlike metagenomics, metatranscriptomics revealed TRF-driven differences in β-diversity (Figure 1D), differential expression (Figures 2A and 2B), and restored diurnal cycling (Figure 3A). These findings confirm our hypothesis and extend previous work by showing that metatranscriptomics not only responds to environmental perturbations[5,15] but also reveals functional shifts associated with host metabolic outcomes. The minimal overlap in differentially expressed or cycling functions detected by metagenomics and metatranscriptomics (Figures 2C and 3C) underscores that gene presence does not reliably predict gene expression—consistent with prior studies of microbial transcriptional regulation relative to abundance.[46,47] Furthermore, while interest in metaproteomics is growing,[48,49] microbial proteins have half-lives ranging from 12 to 42 h,[50] limiting their ability to detect rapid temporal changes. By contrast, microbial RNA degrades within fractions of a minute to an hour,[17] allowing metatranscriptomics to capture fast, dynamic microbial responses. This underscores

metatranscriptomics' ability to provide a deeper, more dynamic view of microbiome activity than other omics methods.

The transcripts restored by TRF primarily pertained to bacterial lipid and carbohydrate metabolism (Figures 2E, 2F, and 3J). In particular, the expression of prokaryotic diacylglycerol kinase and enoyl-ACP reductase—enzymes in lipid signaling and fatty acid metabolism —were significantly lower in TRF mice during the dark phase compared with FA mice, based on both differential expression and cycling analyses. These results suggest that TRF suppresses microbial lipid synthesis in DIO mice, consistent with prior reports of TRF improving obesity phenotypes[1,3] and host transcriptional profiles.[51] These findings further raise the possibility that microbial nutrient metabolism contributes to diet-induced dysmetabolism and should be further explored using tools for functional microbiome manipulation, such as ENBs. While prior metatranscriptomic studies have shown enrichment of carbohydrate, protein, and lipid metabolism pathways in obesity,[20] our data uniquely reveal their temporal modulation by dietary intervention through TRF. By pinpointing bacterial functions that are both diurnally regulated and therapeutically relevant, our findings offer a blueprint for engineering microbial interventions that operate in real time with host physiology.

TRF induced a distinct cycling signature in metatranscriptomics (Figures 3A and 3B), restoring transcripts previously rhythmic under NCD but lost under HFD. These included β-galactosidase, lipoate protein ligase, and glycosyltransferase (Figure S3E)—enzymes associated with weight loss, improved insulin sensitivity, and reduced inflammation.[52–57] TRF also shifted the phase of transcripts that cycled under FA but not NA—such as glycosyl hydrolases and 2-thiouracil desulfuratase, enzymes involved in carbohydrate breakdown and protein translation,[58,59] (Figure S3D)—from the dark to the light phase. This suggests that HFD disrupts the timing and availability of microbial functions, potentially contributing to metabolic dysfunction.

Despite the known diurnal dynamics of the microbiome,[1–3,26] most studies overlook timing in sample collection. We show that TRF-induced changes in microbial composition (16S, Figure 1E) and function (metatranscriptomics, Figure 2B) would have been missed without accounting for the timing of sample collection. This reinforces the principle—known in host transcriptomics—that timing of transcript presence can critically impact physiological outcomes.

Using metatranscriptomics, we uncovered diet- and TRF-specific *bsh* expression patterns at the species level, consistent with prior work demonstrating functional specificity among BSHs.[39,44] We also found that *bsh* expression varies in its diurnal regulation. While *L. gasseri* and *D. newyorkensis bsh* were enriched under HFD and TRF, respectively, only *D. newyorkensis bsh* transcripts exhibited diurnal oscillations (Figures 4D and 4E). *D. newyorkensis* has emerged as a potential therapeutic agent due to its role in colitis amelioration,[60] anti-aging,[61] and metabolic improvement in metabolic dysfunction-associated steatoic liver disease (MASLD) models.[62] These findings suggest *D. newyorkensis bsh* may potentially contribute to the effects of TRF.

In the native *E. coli* chassis, the *D. newyorkensis bsh1* (DnBSH1) demonstrated broader substrate specificity, deconjugating both glycine- and taurine-conjugated BAs, despite having a taurine-preferring motif. This promiscuity may explain its stronger physiological metabolic impact relative to BSHs limited to a single conjugate class. Structural studies of such BSHs could inform the design of precision microbial therapeutics. We also tested amidation activity and discovered that DnBSH1 (from the TRF metatranscriptome) produced multiple BBAAs *in vitro*, while the LgBSH (from DIO) did not (Figures 5E–5H). Although some BBAAs may act as farnesoid X receptor (FXR) agonists,[34,63] their broader interactions with receptors like Takeda G-protein coupled receptor 5 (TGR5), pregnane X receptor (PXR), and aryl hydrocarbon receptor (AhR) remain unknown.[34] Nevertheless, our findings demonstrate that metatranscriptomics can uncover microbial enzymes with distinct substrate profiles and regulatory properties shaped by diet—offering a path to engineer therapeutics targeting diet-sensitive metabolic pathways.

*In vivo*, mice colonized with EcAZ-1$^{DnBSH1}$—the TRF-derived DnBSH1— showed improved glucose regulation, enhanced insulin response, reduced fat mass, and increased lean mass (Figures 6F–6I), mirroring TRF-associated metabolic benefits.[1,6,7] This study demonstrates that an engineered BSH microbe can alter body composition in a non-obese background, a result not previously reported. Since two of the BSHs we engineered were enriched under HFD, we hypothesize that these ENBs may yield similar improvements in HFD-fed mice—though this remains to be tested. These findings suggest that *D. newyorkensis* BSH may contribute to TRF's phenotypic effects and exert greater metabolic benefits than previously characterized BSHs.

Fecal metabolomics provided evidence that these BSH ENBs could modify the luminal BBAA pool. Interestingly, differences in BBAA levels were diurnal, despite the *bsh* genes being under constitutive promoters. This implies that interactions between the ENBs and the host or microbiome circadian rhythms are critical for their activity. Further studies are needed to test this and clarify the role of the gut microbiome–BA axis in metabolic benefits associated with feeding behaviors like TRF. Altogether, our results show that metatranscriptomics enables discovery of potent microbial functions that influence host physiology and opens the door to developing microbial therapies tuned to dietary and temporal contexts.

Limitations of our study include our use of Woltka for annotation, which favors biological relevance but lacks comprehensive coverage. The Web of Life database may underrepresent *bsh* genes, which we addressed by supplementing with a curated BSH database to improve detection. Similarly, Pfam-based annotations limited pathway analyses and hindered species-level comparisons for non-*bsh* genes without further validation. Future studies could build on our dataset to identify other microbial enzymes responsive to TRF. Differences in sequencing depth between metagenomics and metatranscriptomics could pose another challenge. However, even after rarefying the metatranscriptomics data to match the metagenomics depth, we still observed TRF-specific effects not seen in the metagenome, underscoring metatranscriptomics' greater sensitivity. Determining statistical power and sample size in circadian microbiome studies remains challenging because it is less well-characterized than RNA-seq, underscoring the need for further research to define optimal sampling strategies per time point.

Our *in vivo* work focused on 6-week outcomes. Long-term effects and performance in DIO models should be further explored in future studies. Spatial variation in *bsh* expression along the gastrointestinal tract is another factor not assessed here. Lastly, several transcripts annotated as *bsh* (e.g., DnBSH2) lacked enzymatic activity, illustrating a broader issue in microbiome research: functionally distinct genes can share the same annotation, complicating predictions of microbial activity.

In this study, we demonstrated that metatranscriptomics can capture time-sensitive microbial changes driven by TRF and can be used to guide microbial engineering. We show that this approach led to the development of a BSH-expressing ENB with stronger metabolic effects than previously reported strains. Metatranscriptomics is thus a powerful platform for understanding dynamic microbial functions and for creating the next generation of personalized LBTs.

## RESOURCE AVAILABILITY

### Lead contact

Further information and requests for resources should be directed to and will be fulfilled by the lead contact, Amir Zarrinpar (azarrinpar@ucsd.edu).

### Materials availability

EcAZ-1-cat, EcAZ-1$^{DnBSH1}$, EcAZ-1$^{DnBSH2}$, EcAZ-1$^{LgBSH}$, EcAZ-1$^{LCAG95BSH}$, and EcAZ-1$^{EpBSH}$ will be made available subject to a materials transfer agreement with the University of California, San Diego.

### Data and code availability

Metatranscriptomics and metagenomics data have been deposited under ENA project PRJEB89098 and are publicly available as of the date of publication. Metabolomics data were uploaded to massive.ucsd.edu and can be accessed using the following identifiers: MSV000094578 and MSV000097414. All original code has been deposited at Mendeley Data, V1, https://doi.org/10.17632/r3t9jm798y.1, and https://github.com/ZarrinparLab/TRF-metaT and is publicly available as of the date of publication. Any additional information required to reanalyze the data reported in this paper is available from the lead contact upon request.

## ACKNOWLEDGMENTS

The authors wish to thank Steven D. Brown for his contribution to the metagenomic and metatranscriptomic sequencing strategy during the early phases of this study. S.F.R. is supported by the Paul & Daisy Soros Foundation. N.S. is supported by NSF GRFP 1000340660. A.L. is supported by the American Heart Association 24POST1199418. P.C.D. acknowledges support by R01DK136117. R.K. also receives funding from NIH U24CA248454 and NIH DP1AT010885. S.P. is supported by R01 CA236352, R01 CA258221, and the Joe Tsai and Clara Wu Foundation. A.Z. and J.H. are supported by NIH R01 EB030134. A.Z., J.H., and R.K. are supported by R01 AI163483. A.Z. is further supported by NIH R01 HL148801, U01 CA265719, and VA Merit BLR&D award I01 BX005707. All authors receive institutional support from NIH P30 DK120515, P30 DK063491, P30 CA014195, P50 AA011999, and UL1 TR001442.

## AUTHOR CONTRIBUTIONS

S.P. and A.Z. conceptualized the project, and S.F.R. and A.Z. designed the analysis. S.F.R. and R.A.R. processed the data. S.F.R. analyzed the results. A.L.L. provided a curated BSH protein database. N.S. led the engineering and *in vitro* bacterial experiments. P.C.D., I.M., W.D.G.N., and J.Z. were responsible for the untargeted metabolomics and BA analysis. W.Z. led the *in vivo* mouse experiments. S.F.R. wrote the original draft of the manuscript. S.F.R., A.L., and A.Z. wrote and edited the manuscript. S.K., Q.Z., Z.Z.X., J. H., S.P., R.K., and P.C.D. provided critical intellectual input. All authors had access to data for the study. A.Z. supervised the study and is ultimately responsible for its content.

## DECLARATION OF INTERESTS

A.Z. is a co-founder and acting CMO of Endure Biotherapeutics. He holds equity in the company. S.P. is a co-founder of Circadian Biosystems and is an author of the books "The Circadian Code" and "The Circadian Diabetes Code." J.H. is a co-founder of GenCirq Inc, which focuses on cancer therapeutics. He is on the Board of Directors and has equity in GenCirq. His spouse is employed part time for bookkeeping and to support employees with human resources. P.C.D. is an adviser and holds equity in Cybele, BileOmix, and Sirenas and is a scientific co-founder and adviser and holds equity in Ometa, Enveda, and Arome with prior approval by UC San Diego. P.C.D. also consulted for DSM animal health in 2023. R.K. is a scientific advisory board member and consultant for BiomeSense, Inc. and has equity and receives income. He is a scientific advisory board member and has equity in GenCirq. He has equity in and acts as a consultant for Cybele. He is a co-founder of Biota, Inc., and has equity. He is a co-founder of Micronoma and has equity and is a scientific advisory board member. The terms of these arrangements have been reviewed and approved by the University of California, San Diego in accordance with its conflict-of-interest policies.

## DECLARATION OF GENERATIVE AI AND AI-ASSISTED TECHNOLOGIES IN THE WRITING PROCESS

During the preparation of this work, the authors S.F.R. and A.Z. used ChatGPT-3.5/ChatGPT-4o to improve the clarity and readability of this manuscript. After using this tool, all authors reviewed and edited the content as needed and take full responsibility for the content of the published article.

## STAR★METHODS

Detailed methods are provided in the online version of this paper and include the following:

- KEY RESOURCES TABLE
- EXPERIMENTAL MODEL AND STUDY PARTICIPANT DETAILS
  - HFD and TRF animal experiment
  - ENB *in vivo* animal experiment
- METHOD DETAILS
  - Microbial Engineering
  - Bile Acid quantification *in vitro*
  - Bacterial colonization and BSH activity
  - Blood glucose and insulin quantification
  - Fat and lean mass quantification
- QUANTIFICATION AND STATISTICAL ANALYSIS
  - 16S data processing
  - Metatranscriptomics sample and data processing
  - Metagenomics sample and data processing
  - Diversity analysis
  - Differential expression
  - Cycling analysis
  - *bsh* expression analysis
  - LC-MS/MS sample processing and data acquisition
  - BSH protein sequence characterization

## SUPPLEMENTAL INFORMATION

Supplemental information can be found online at https://doi.org/10.1016/j.chom.2025.05.024.

Received: November 7, 2024
Revised: March 24, 2025
Accepted: May 23, 2025
Published: June 18, 2025

## REFERENCES


1. Zarrinpar, A., Chaix, A., Yooseph, S., and Panda, S. (2014). Diet and feeding pattern affect the diurnal dynamics of the gut microbiome. Cell Metab. *20*, 1006–1017. https://doi.org/10.1016/j.cmet.2014.11.008.
2. Leone, V., Gibbons, S.M., Martinez, K., Hutchison, A.L., Huang, E.Y., Cham, C.M., Pierre, J.F., Heneghan, A.F., Nadimpalli, A., Hubert, N., et al. (2015). Effects of diurnal variation of gut microbes and high-fat feeding on host circadian clock function and metabolism. Cell Host Microbe *17*, 681–689. https://doi.org/10.1016/j.chom.2015.03.006.
3. Dantas Machado, A.C., Brown, S.D., Lingaraju, A., Sivaganesh, V., Martino, C., Chaix, A., Zhao, P., Pinto, A.F.M., Chang, M.W., Richter, R. A., et al. (2022). Diet and feeding pattern modulate diurnal dynamics of the ileal microbiome and transcriptome. Cell Rep. *40*, 111008. https://doi.org/10.1016/j.celrep.2022.111008.
4. Thaiss, C.A., Zeevi, D., Levy, M., Zilberman-Schapira, G., Suez, J., Tengeler, A.C., Abramson, L., Katz, M.N., Korem, T., Zmora, N., et al. (2014). Transkingdom control of microbiota diurnal oscillations promotes metabolic homeostasis. Cell *159*, 514–529. https://doi.org/10.1016/j.cell.2014.09.048.
5. Maurice, C.F., Haiser, H.J., and Turnbaugh, P.J. (2013). Xenobiotics Shape the Physiology and Gene Expression of the Active Human Gut Microbiome. Cell *152*, 39–50. https://doi.org/10.1016/j.cell.2012.10.052.
6. Petersen, M.C., Gallop, M.R., Flores Ramos, S., Zarrinpar, A., Broussard, J.L., Chondronikola, M., Chaix, A., and Klein, S. (2022). Complex physiology and clinical implications of time-restricted eating. Physiol. Rev. *102*, 1991–2034. https://doi.org/10.1152/physrev.00006.2022.
7. Hatori, M., Vollmers, C., Zarrinpar, A., DiTacchio, L., Bushong, E.A., Gill, S., Leblanc, M., Chaix, A., Joens, M., Fitzpatrick, J.A.J., et al. (2012). Time-restricted feeding without reducing caloric intake prevents metabolic diseases in mice fed a high-fat diet. Cell Metab. *15*, 848–860. https://doi.org/10.1016/j.cmet.2012.04.019.
8. Chaix, A., Zarrinpar, A., Miu, P., and Panda, S. (2014). Time-Restricted Feeding Is a Preventative and Therapeutic Intervention against Diverse Nutritional Challenges. Cell Metab. *20*, 991–1005. https://doi.org/10.1016/j.cmet.2014.11.001.
9. Saran, A.R., Dave, S., and Zarrinpar, A. (2020). Circadian Rhythms in the Pathogenesis and Treatment of Fatty Liver Disease. Gastroenterology *158*, 1948–1966.e1. https://doi.org/10.1053/j.gastro.2020.01.050.
10. Russell, B.J., Brown, S.D., Siguenza, N., Mai, I., Saran, A.R., Lingaraju, A., Maissy, E.S., Dantas Machado, A.C., Pinto, A.F.M., Sanchez, C., et al. (2022). Intestinal transgene delivery with native E. coli chassis allows persistent physiological changes. Cell *185*, 3263–3277.e15. https://doi.org/10.1016/j.cell.2022.06.050.
11. Joyce, S.A., MacSharry, J., Casey, P.G., Kinsella, M., Murphy, E.F., Shanahan, F., Hill, C., and Gahan, C.G.M. (2014). Regulation of host weight gain and lipid metabolism by bacterial bile acid modification in the gut. Proc. Natl. Acad. Sci. USA *111*, 7421–7426. https://doi.org/10.1073/pnas.1323599111.
12. Shakya, M., Lo, C.-C., and Chain, P.S.G. (2019). Advances and Challenges in Metatranscriptomic Analysis. Front. Genet. *10*, 904. https://doi.org/10.3389/fgene.2019.00904.
13. Bashiardes, S., Zilberman-Schapira, G., and Elinav, E. (2016). Use of metatranscriptomics in microbiome research. Bioinformatics Biol. Insights *10*, 19–25. https://doi.org/10.4137/BBI.S34610.
14. Franzosa, E.A., McIver, L.J., Rahnavard, G., Thompson, L.R., Schirmer, M., Weingart, G., Lipson, K.S., Knight, R., Caporaso, J.G., Segata, N., et al. (2018). Species-level functional profiling of metagenomes and metatranscriptomes. Nat. Methods *15*, 962–968. https://doi.org/10.1038/s41592-018-0176-y.
15. David, L.A., Maurice, C.F., Carmody, R.N., Gootenberg, D.B., Button, J.E., Wolfe, B.E., Ling, A.V., Devlin, A.S., Varma, Y., Fischbach, M.A., et al. (2014). Diet rapidly and reproducibly alters the human gut microbiome. Nature *505*, 559–563. https://doi.org/10.1038/nature12820.
16. Ojala, T., Kankuri, E., and Kankainen, M. (2023). Understanding human health through metatranscriptomics. Trends Mol. Med. *29*, 376–389. https://doi.org/10.1016/j.molmed.2023.02.002.
17. Belasco, J.G. (2010). All things must pass: contrasts and commonalities in eukaryotic and bacterial mRNA decay. Nat. Rev. Mol. Cell Biol. *11*, 467–478. https://doi.org/10.1038/nrm2917.
18. Abu-Ali, G.S., Mehta, R.S., Lloyd-Price, J., Mallick, H., Branck, T., Ivey, K. L., Drew, D.A., DuLong, C., Rimm, E., Izard, J., et al. (2018). Metatranscriptome of human faecal microbial communities in a cohort of adult men. Nat. Microbiol. *3*, 356–366. https://doi.org/10.1038/s41564-017-0084-4.
19. Schirmer, M., Franzosa, E.A., Lloyd-Price, J., McIver, L.J., Schwager, R., Poon, T.W., Ananthakrishnan, A.N., Andrews, E., Barron, G., Lake, K., et al. (2018). Dynamics of metatranscription in the inflammatory bowel disease gut microbiome. Nat. Microbiol. *3*, 337–346. https://doi.org/10.1038/s41564-017-0089-z.
20. Granata, I., Nardelli, C., D'Argenio, V., Tramontano, S., Compare, D., Guarracino, M.R., Nardone, G., Pilone, V., and Sacchetti, L. (2020). Duodenal Metatranscriptomics to Define Human and Microbial Functional Alterations Associated with Severe Obesity: A Pilot Study. Microorganisms *8*, 1811. https://doi.org/10.3390/microorganisms8111811.
21. Jain, V., Baraniya, D., El-Hadedy, D.E., Chen, T., Slifker, M., Alakwaa, F., Cai, K.Q., Chitrala, K.N., Fundakowski, C., and Al-Hebshi, N.N. (2023). Integrative Metatranscriptomic Analysis Reveals Disease-specific Microbiome–host Interactions in Oral Squamous Cell Carcinoma. Cancer Res. Commun. *3*, 807–820. https://doi.org/10.1158/2767-9764.CRC-22-0349.
22. Heintz-Buschart, A., May, P., Laczny, C.C., Lebrun, L.A., Bellora, C., Krishna, A., Wampach, L., Schneider, J.G., Hogan, A., De Beaufort, C., et al. (2016). Integrated multi-omics of the human gut microbiome in a case study of familial type 1 diabetes. Nat. Microbiol. *2*, 16180. https://doi.org/10.1038/nmicrobiol.2016.180.
23. Bae, M., Le, C., Mehta, R.S., Dong, X., Pieper, L.M., Ramirez, L., Alexander, M., Kiamehr, S., Turnbaugh, P.J., Huttenhower, C., et al. (2024). Metatranscriptomics-guided discovery and characterization of a polyphenol-metabolizing gut microbial enzyme. Cell Host Microbe *32*, 1887–1896.e8. https://doi.org/10.1016/j.chom.2024.10.002.
24. Fernandes, A.D., Reid, J.N., Macklaim, J.M., McMurrough, T.A., Edgell, D. R., and Gloor, G.B. (2014). Unifying the analysis of high-throughput sequencing datasets: characterizing RNA-seq, 16S rRNA gene sequencing and selective growth experiments by compositional data analysis. Microbiome *2*, 15. https://doi.org/10.1186/2049-2618-2-15.
25. Nearing, J.T., Douglas, G.M., Hayes, M.G., MacDonald, J., Desai, D.K., Allward, N., Jones, C.M.A., Wright, R.J., Dhanani, A.S., Comeau, A.M., et al. (2022). Microbiome differential abundance methods produce different results across 38 datasets. Nat. Commun. *13*, 342. https://doi.org/10.1038/s41467-022-28034-z.
26. Allaband, C., Lingaraju, A., Flores Ramos, S., Kumar, T., Javaheri, H., Tiu, M.D., Dantas Machado, A.C., Richter, R.A., Elijah, E., Haddad, G.G., et al. (2024). Time of sample collection is critical for the replicability of microbiome analyses. Nat. Metab. *6*, 1282–1293. https://doi.org/10.1038/s42255-024-01064-1.
27. Massengo-Tiassé, R.P., and Cronan, J.E. (2009). Diversity in enoyl-acyl carrier protein reductases. Cell. Mol. Life Sci. *66*, 1507–1517. https://doi.org/10.1007/s00018-009-8704-7.
28. Massart, J., and Zierath, J.R. (2019). Role of Diacylglycerol Kinases in Glucose and Energy Homeostasis. Trends Endocrinol. Metab. *30*, 603–617. https://doi.org/10.1016/j.tem.2019.06.003.
29. García-Fontana, C., Reyes-Darias, J.A., Muñoz-Martínez, F., Alfonso, C., Morel, B., Ramos, J.L., and Krell, T. (2013). High Specificity in CheR Methyltransferase Function: CheR2 of Pseudomonas putida is essential for chemotaxis, whereas CheR1 is involved in biofilm formation. J. Biol. Chem. *288*, 18987–18999. https://doi.org/10.1074/jbc.M113.472605.

30. Thoden, J.B., and Holden, H.M. (2007). The molecular architecture of glucose-1-phosphate uridylyltransferase. Protein Sci. *16*, 432–440. https://doi.org/10.1110/ps.062626007.

31. Swigoňová, Z., Mohsen, A.-W., and Vockley, J. (2009). Acyl-CoA Dehydrogenases: Dynamic History of Protein Family Evolution. J. Mol. Evol. *69*, 176–193. https://doi.org/10.1007/s00239-009-9263-0.

32. Yu, J., Loh, K., Song, Z.Y., Yang, H.Q., Zhang, Y., and Lin, S. (2018). Update on glycerol-3-phosphate acyltransferases: the roles in the development of insulin resistance. Nutr. Diabetes *8*, 34. https://doi.org/10.1038/s41387-018-0045-x.

33. Kapoor, M., Reddy, C.C., Krishnasastry, M.V., Surolia, N., and Surolia, A. (2004). Slow-tight-binding inhibition of enoyl-acyl carrier protein reductase from Plasmodium falciparum by triclosan. Biochem. J. *381*, 719–724. https://doi.org/10.1042/BJ20031821.

34. Rimal, B., Collins, S.L., Tanes, C.E., Rocha, E.R., Granda, M.A., Solanki, S., Hoque, N.J., Gentry, E.C., Koo, I., Reilly, E.R., et al. (2024). Bile salt hydrolase catalyses formation of amine-conjugated bile acids. Nature *626*, 859–863. https://doi.org/10.1038/s41586-023-06990-w.

35. Frazier, K., and Chang, E.B. (2020). Intersection of the Gut Microbiome and Circadian Rhythms in Metabolism. Trends Endocrinol. Metab. *31*, 25–36. https://doi.org/10.1016/j.tem.2019.08.013.

36. Gutierrez Lopez, D.E., Lashinger, L.M., Weinstock, G.M., and Bray, M.S. (2021). Circadian rhythms and the gut microbiome synchronize the host's metabolic response to diet. Cell Metab. *33*, 873–887. https://doi.org/10.1016/j.cmet.2021.03.015.

37. Govindarajan, K., MacSharry, J., Casey, P.G., Shanahan, F., Joyce, S.A., and Gahan, C.G.M. (2016). Unconjugated Bile Acids Influence Expression of Circadian Genes: A Potential Mechanism for Microbe-Host Crosstalk. PLoS One *11*, e0167319. https://doi.org/10.1371/journal.pone.0167319.

38. Rahman, G., Morton, J.T., Martino, C., Sepich-Poore, G.D., Allaband, C., Guccione, C., Chen, Y., Hakim, D., Estaki, M., and Knight, R. (2023). BIRDMAn: A Bayesian differential abundance framework that enables robust inference of host-microbe associations. Preprint at bioRxiv. https://doi.org/10.1101/2023.01.30.526328.

39. Foley, M.H., O'Flaherty, S., Allen, G., Rivera, A.J., Stewart, A.K., Barrangou, R., and Theriot, C.M. (2021). Lactobacillus bile salt hydrolase substrate specificity governs bacterial fitness and host colonization. Proc. Natl. Acad. Sci. USA *118*, e2017709118. https://doi.org/10.1073/pnas.2017709118.

40. Bourgin, M., Kriaa, A., Mkaouar, H., Mariaule, V., Jablaoui, A., Maguin, E., and Rhimi, M. (2021). Bile Salt Hydrolases: At the Crossroads of Microbiota and Human Health. Microorganisms *9*, 1122. https://doi.org/10.3390/microorganisms9061122.

41. Siguenza, N., Russell, B.J., Richter, R.A., and Zarrinpar, A. (2023). Complete Genome Sequence of an Escherichia coli Strain Isolated from Laboratory Mouse Stool for Use as a Chassis for Transgene Delivery to the Murine Microbiome. Microbiol. Resour. Announc. *12*, e0101422. https://doi.org/10.1128/mra.01014-22.

42. Zarrinpar, A., Chaix, A., Xu, Z.Z., Chang, M.W., Marotz, C.A., Saghatelian, A., Knight, R., and Panda, S. (2018). Antibiotic-induced microbiome depletion alters metabolic homeostasis by affecting gut signaling and colonic metabolism. Nat. Commun. *9*, 2872. https://doi.org/10.1038/s41467-018-05336-9.

43. Jones, B.V., Begley, M., Hill, C., Gahan, C.G.M., and Marchesi, J.R. (2008). Functional and comparative metagenomic analysis of bile salt hydrolase activity in the human gut microbiome. Proc. Natl. Acad. Sci. USA *105*, 13580–13585. https://doi.org/10.1073/pnas.0804437105.

44. Foley, M.H., Walker, M.E., Stewart, A.K., O'Flaherty, S., Gentry, E.C., Patel, S., Beaty, V.V., Allen, G., Pan, M., Simpson, J.B., et al. (2023). Bile salt hydrolases shape the bile acid landscape and restrict Clostridioides difficile growth in the murine gut. Nat. Microbiol. *8*, 611–628. https://doi.org/10.1038/s41564-023-01337-7.

45. Mohanty, I., Allaband, C., Mannochio-Russo, H., El Abiead, Y., Hagey, L. R., Knight, R., and Dorrestein, P.C. (2024). The changing metabolic landscape of bile acids – keys to metabolism and immune regulation. Nat. Rev. Gastroenterol. Hepatol. *21*, 493–516. https://doi.org/10.1038/s41575-024-00914-3.

46. Bikel, S., Valdez-Lara, A., Cornejo-Granados, F., Rico, K., Canizales-Quinteros, S., Soberón, X., Del Pozo-Yauner, L., and Ochoa-Leyva, A. (2015). Combining metagenomics, metatranscriptomics and viromics to explore novel microbial interactions: towards a systems-level understanding of human microbiome. Comp. Struct. Biotechnol. J. *13*, 390–401. https://doi.org/10.1016/j.csbj.2015.06.001.

47. Jovel, J., Nimaga, A., Jordan, T., O'Keefe, S., Patterson, J., Thiesen, A., Hotte, N., Bording-Jorgensen, M., Subedi, S., Hamilton, J., et al. (2022). Metagenomics Versus Metatranscriptomics of the Murine Gut Microbiome for Assessing Microbial Metabolism During Inflammation. Front. Microbiol. *13*, 829378. https://doi.org/10.3389/fmicb.2022.829378.

48. Sun, Z., Ning, Z., and Figeys, D. (2024). The Landscape and Perspectives of the Human Gut Metaproteomics. Mol. Cell. Proteomics *23*, 100763. https://doi.org/10.1016/j.mcpro.2024.100763.

49. Zhang, X., Ning, Z., Mayne, J., and Figeys, D. (2025). Clinical Microbiome Analysis by Mass Spectrometry-Based Metaproteomics. Annu. Rev. Anal. Chem. (Palo Alto. Calif) *18*, 149–172. https://doi.org/10.1146/annurev-anchem-071124-113819.

50. Maier, T., Schmidt, A., Güell, M., Kühner, S., Gavin, A.C., Aebersold, R., and Serrano, L. (2011). Quantification of mRNA and protein and integration with protein turnover in a bacterium. Mol. Syst. Biol. *7*, 511. https://doi.org/10.1038/msb.2011.38.

51. Deota, S., Lin, T., Chaix, A., Williams, A., Le, H., Calligaro, H., Ramasamy, R., Huang, L., and Panda, S. (2023). Diurnal transcriptome landscape of a multi-tissue response to time-restricted feeding in mammals. Cell Metab. *35*, 150–165.e4. https://doi.org/10.1016/j.cmet.2022.12.006.

52. Zhang, R., Yip, V.L.Y., and Withers, S.G. (2010). Mechanisms of Enzymatic Glycosyl Transfer. Comprehensive Natural Products II, H.-W. (Ben) Liu and L. Mander, eds. (Elsevier), pp. 385–422.

53. Reily, C., Stewart, T.J., Renfrow, M.B., and Novak, J. (2019). Glycosylation in health and disease. Nat. Rev. Nephrol. *15*, 346–366. https://doi.org/10.1038/s41581-019-0129-4.

54. Li, Y., Huang, J., Zhang, S., Yang, F., Zhou, H., Song, Y., Wang, B., and Li, H. (2022). Sodium alginate and galactooligosaccharides ameliorate metabolic disorders and alter the composition of the gut microbiota in mice with high-fat diet-induced obesity. Int. J. Biol. Macromol. *215*, 113–122. https://doi.org/10.1016/j.ijbiomac.2022.06.073.

55. Mistry, R.H., Liu, F., Borewicz, K., Lohuis, M.A.M., Smidt, H., Verkade, H. J., and Tietge, U.J.F. (2020). Long-Term β-galacto-oligosaccharides Supplementation Decreases the Development of Obesity and Insulin Resistance in Mice Fed a Western-Type Diet. Mol. Nutr. Food Res. *64*, e1900922. https://doi.org/10.1002/mnfr.201900922.

56. Zhu, K., Chen, H., Jin, J., Wang, N., Ma, G., Huang, J., Feng, Y., Xin, J., Zhang, H., and Liu, H. (2020). Functional Identification and Structural Analysis of a New Lipoate Protein Ligase in Mycoplasma hyopneumoniae. Front. Cell. Infect. Microbiol. *10*, 156. https://doi.org/10.3389/fcimb.2020.00156.

57. Tanabe, T.S., Grosser, M., Hahn, L., Kümpel, C., Hartenfels, H., Vtulkin, E., Flegler, W., and Dahl, C. (2023). Identification of a novel lipoic acid biosynthesis pathway reveals the complex evolution of lipoate assembly in prokaryotes. PLoS Biol. *21*, e3002177. https://doi.org/10.1371/journal.pbio.3002177.

58. Amin, K., Tranchimand, S., Benvegnu, T., Abdel-Razzak, Z., and Chamieh, H. (2021). Glycoside Hydrolases and Glycosyltransferases from Hyperthermophilic Archaea: Insights on Their Characteristics and Applications in Biotechnology. Biomolecules *11*, 1557. https://doi.org/10.3390/biom11111557.

59. Fuchs, J., Jamontas, R., Hoock, M.H., Oltmanns, J., Golinelli-Pimpaneau, B., Schünemann, V., Pierik, A.J., Meškys, R., Aučynaitė, A., and Boll, M. (2023). TudS desulfidases recycle 4-thiouridine-5′-monophosphate at a catalytic [4Fe-4S] cluster. Commun. Biol. *6*, 1092. https://doi.org/10.1038/s42003-023-05450-5.

60. Zhang, Y., Tu, S., Ji, X., Wu, J., Meng, J., Gao, J., Shao, X., Shi, S., Wang, G., Qiu, J., et al. (2024). Dubosiella newyorkensis modulates immune tolerance in colitis via the L-lysine-activated AhR-IDO1-Kyn pathway. Nat. Commun. *15*, 1333. https://doi.org/10.1038/s41467-024-45636-x.

61. Liu, T.H., Wang, J., Zhang, C.Y., Zhao, L., Sheng, Y.Y., Tao, G.S., and Xue, Y.Z. (2023). Gut microbial characteristical comparison reveals potential anti-aging function of Dubosiella newyorkensis in mice. Front. Endocrinol. *14*, 1133167. https://doi.org/10.3389/fendo.2023.1133167.

62. Lin, Y.-N., Hsu, J.-R., Wang, C.-L., Huang, Y.-C., Wang, J.-Y., Wu, C.-Y., and Wu, L.-L. (2024). Nuclear factor interleukin 3 and metabolic dysfunction-associated fatty liver disease development. Commun. Biol. *7*, 897. https://doi.org/10.1038/s42003-024-06565-z.

63. Quinn, R.A., Melnik, A.V., Vrbanac, A., Fu, T., Patras, K.A., Christy, M.P., Bodai, Z., Belda-Ferre, P., Tripathi, A., Chung, L.K., et al. (2020). Global chemical effects of the microbiome include new bile-acid conjugations. Nature *579*, 123–129. https://doi.org/10.1038/s41586-020-2047-9.

64. Langmead, B., and Salzberg, S.L. (2012). Fast gapped-read alignment with Bowtie 2. Nat. Methods *9*, 357–359. https://doi.org/10.1038/nmeth.1923.

65. Nawrocki, E.P., and Eddy, S.R. (2013). Infernal 1.1: 100-fold faster RNA homology searches. Bioinformatics *29*, 2933–2935. https://doi.org/10.1093/bioinformatics/btt509.

66. Zhu, Q., Huang, S., Gonzalez, A., McGrath, I., McDonald, D., Haiminen, N., Armstrong, G., Vázquez-Baeza, Y., Yu, J., Kuczynski, J., et al. (2022). Phylogeny-Aware Analysis of Metagenome Community Ecology Based on Matched Reference Genomes while Bypassing Taxonomy. mSystems *7*, e0016722. https://doi.org/10.1128/msystems.00167-22.

67. Bolyen, E., Rideout, J.R., Dillon, M.R., Bokulich, N.A., Abnet, C.C., Al-Ghalith, G.A., Alexander, H., Alm, E.J., Arumugam, M., Asnicar, F., et al. (2019). Reproducible, interactive, scalable and extensible microbiome data science using QIIME 2. Nat. Biotechnol. *37*, 852–857. https://doi.org/10.1038/s41587-019-0209-9.

68. Wu, G., Anafi, R.C., Hughes, M.E., Kornacker, K., and Hogenesch, J.B. (2016). MetaCycle: An integrated R package to evaluate periodicity in large scale data. Bioinformatics *32*, 3351–3353. https://doi.org/10.1093/bioinformatics/btw405.

69. Buchfink, B., Xie, C., and Huson, D.H. (2015). Fast and sensitive protein alignment using DIAMOND. Nat. Methods *12*, 59–60. https://doi.org/10.1038/nmeth.3176.

70. Schmid, R., Heuckeroth, S., Korf, A., Smirnov, A., Myers, O., Dyrlund, T.S., Bushuiev, R., Murray, K.J., Hoffmann, N., Lu, M., et al. (2023). Integrative analysis of multimodal mass spectrometry data in MZmine 3. Nat. Biotechnol. *41*, 447–449. https://doi.org/10.1038/s41587-023-01690-2.

71. Nothias, L.F., Petras, D., Schmid, R., Dührkop, K., Rainer, J., Sarvepalli, A., Protsyuk, I., Ernst, M., Tsugawa, H., Fleischauer, M., et al. (2020). Feature-based molecular networking in the GNPS analysis environment. Nat. Methods *17*, 905–908. https://doi.org/10.1038/s41592-020-0933-6.

72. Wang, M., Carver, J.J., Phelan, V.V., Sanchez, L.M., Garg, N., Peng, Y., Nguyen, D.D., Watrous, J., Kapono, C.A., Luzzatto-Knaan, T., et al. (2016). Sharing and community curation of mass spectrometry data with Global Natural Products Social Molecular Networking. Nat. Biotechnol. *34*, 828–837. https://doi.org/10.1038/nbt.3597.

73. Sievers, F., Wilm, A., Dineen, D., Gibson, T.J., Karplus, K., Li, W., Lopez, R., McWilliam, H., Remmert, M., Söding, J., et al. (2011). Fast, scalable generation of high-quality protein multiple sequence alignments using Clustal Omega. Mol. Syst. Biol. *7*, 539. https://doi.org/10.1038/msb.2011.75.

74. Schurch, N.J., Schofield, P., Gierliński, M., Cole, C., Sherstnev, A., Singh, V., Wrobel, N., Gharbi, K., Simpson, G.G., Owen-Hughes, T., et al. (2016). How many biological replicates are needed in an RNA-seq experiment and which differential expression tool should you use? RNA *22*, 839–851. https://doi.org/10.1261/rna.053959.115.

75. Bassalo, M.C., Garst, A.D., Halweg-Edwards, A.L., Grau, W.C., Domaille, D.W., Mutalik, V.K., Arkin, A.P., and Gill, R.T. (2016). Rapid and Efficient One-Step Metabolic Pathway Integration in E. coli. ACS Synth. Biol. *5*, 561–568. https://doi.org/10.1021/acssynbio.5b00187.

76. Zhu, Q., Mai, U., Pfeiffer, W., Janssen, S., Asnicar, F., Sanders, J.G., Belda-Ferre, P., Al-Ghalith, G.A., Kopylova, E., McDonald, D., et al. (2019). Phylogenomics of 10,575 genomes reveals evolutionary proximity between domains Bacteria and Archaea. Nat. Commun. *10*, 5477. https://doi.org/10.1038/s41467-019-13443-4.

77. Hakim, D., Wandro, S., Zengler, K., Zaramela, L.S., Nowinski, B., Swafford, A., Zhu, Q., Song, S.J., Gonzalez, A., McDonald, D., et al. (2022). Zebra: Static and Dynamic Genome Cover Thresholds with Overlapping References. mSystems *7*, e0075822. https://doi.org/10.1128/msystems.00758-22.

78. Martino, C., Morton, J.T., Marotz, C.A., Thompson, L.R., Tripathi, A., Knight, R., and Zengler, K. (2019). A Novel Sparse Compositional Technique Reveals Microbial Perturbations. mSystems *4*, e0001619. https://doi.org/10.1128/mSystems.00016-19.

79. Wickham, H. (2016). ggplot2: Elegant Graphics for Data Analysis. In ggplot2: Elegant Graphics for Data Analysis, H. Wickham, ed. (Springer International Publishing), pp. 189–201.

80. Gerlt, J.A., Bouvier, J.T., Davidson, D.B., Imker, H.J., Sadkhin, B., Slater, D.R., and Whalen, K.L. (2015). Enzyme Function Initiative-Enzyme Similarity Tool (EFI-EST): A web tool for generating protein sequence similarity networks. Biochim. Biophys. Acta *1854*, 1019–1037. https://doi.org/10.1016/j.bbapap.2015.04.015.

81. Mohanty, I., Mannochio-Russo, H., Schweer, J.V., El Abiead, Y.E., Bittremieux, W., Xing, S., Schmid, R., Zuffa, S., Vasquez, F., Muti, V.B., et al. (2024). The underappreciated diversity of bile acid modifications. Cell *187*, 1801–1818.e20. https://doi.org/10.1016/j.cell.2024.02.019.

82. Adams, K.J., Pratt, B., Bose, N., Dubois, L.G., St John-Williams, L., Perrott, K.M., Ky, K., Kapahi, P., Sharma, V., MacCoss, M.J., et al. (2020). Skyline for Small Molecules: A Unifying Software Package for Quantitative Metabolomics. J. Proteome Res. *19*, 1447–1458. https://doi.org/10.1021/acs.jproteome.9b00640.

83. Kolde, R. (2010). pheatmap: Pretty Heatmaps. https://doi.org/10.32614/CRAN.package.pheatmap.

84. The UniProt Consortium (2023). UniProt: the Universal Protein Knowledgebase in 2023. Nucleic Acids Res. *51*, D523–D531. https://doi.org/10.1093/nar/gkac1052.

## STAR★METHODS

### KEY RESOURCES TABLE

| REAGENT or RESOURCE | SOURCE | IDENTIFIER |
|---|---|---|
| Bacterial and virus strains | | |
| *Escherichia coli* EcAZ-2$^{BSH+}$ | Russell et al.[10] | N/A |
| *Escherichia coli* EcAZ-1-cat | This manuscript | N/A |
| *Escherichia coli* EcAZ-1$^{DnBSH1}$ | This manuscript | N/A |
| *Escherichia coli* EcAZ-1$^{DnBSH2}$ | This manuscript | N/A |
| *Escherichia coli* EcAZ-1$^{LgBSH}$ | This manuscript | N/A |
| *Escherichia coli* EcAZ-1$^{EpBSH}$ | This manuscript | N/A |
| *Escherichia coli* EcAZ-1$^{LCAG95BSH}$ | This manuscript | N/A |
| Biological samples | | |
| HFD and TRF mouse cecal tissue | Zarrinpar et al.[1] | N/A |
| ENB treated mouse fecal samples | This manuscript | N/A |
| ENB treated mouse blood samples | This manuscript | N/A |
| Chemicals, peptides, and recombinant proteins | | |
| Glycocholic acid (GCA) | Sigma Aldrich | Cat# 475-31-0 |
| Glycochenodeoxycholic acid (GCDCA) | Sigma Aldrich | Cat# 640-79-9 |
| Glycodeoxycholic acid (GDCA) | Sigma Aldrich | Cat# 360-65-6 |
| Glycolithocholic acid (GLCA) | Sigma Aldrich | Cat# 474-74-8 |
| Glycoursodeoxycholic acid (GUDCA) | Sigma Aldrich | Cat# 64480-66-6 |
| Taurocholic acid (TCA) | Sigma Aldrich | Cat# 145-42-6 |
| Taurochenodeoxycholic acid (TCDCA) | Sigma Aldrich | Cat# 6009-98-9 |
| Taurodeoxycholic acid (TDCA) | Sigma Aldrich | Cat# 1180-95-6 |
| Taurolithocholic acid (TLCA) | Sigma Aldrich | Cat# 6042-32-6 |
| Tauroursodeoxycholic acid (TUDCA) | Sigma Aldrich | Cat# 35807-85-3 |
| TRIzol Reagent | Life Technologies | Cat# 15596026 |
| Critical commercial assays | | |
| PureLink RNA mini kit | Life Technologies | Cat# 12183025 |
| Ribo-Zero kit | Illumina | Cat# 20037135 |
| Ultra Sensitive Mouse insulin ELISA Kit | Crystal Chem | Cat# 90080 |
| Deposited data | | |
| HFD and TRF mouse weight and blood glucose data | Zarrinpar et al.[1] | Mendeley Data, V1, https://doi.org/10.17632/xyxpvsyvzn.1 |
| Cecal 16S amplicon sequencing data | Zarrinpar et al.[1] | Satchidananda Panda Lab |
| Cecal shotgun metagenomic sequencing data | This manuscript | PRJEB89098 |
| Cecal metatranscriptomic sequencing data | This manuscript | PRJEB89098 |
| Ileum targeted metabolomics data for bile acids | Machado et al.[3] | Mendeley Data, V1, https://doi.org/10.17632/xyxpvsyvzn.1 |
| ENB culture untargeted metabolomics data | This manuscript | MSV000094578 |
| ENB *in vivo* fecal untargeted metabolomics data | This manuscript | MSV000097414 |
| ENB *in vivo* serum insulin and glucose data | This manuscript | Mendeley Data, V1, https://doi.org/10.17632/r3t9jm798y.1 |
| ENB *in vivo* body composition (fat and lean mass) | This manuscript | Mendeley Data, V1, https://doi.org/10.17632/r3t9jm798y.1 |
| Experimental models: Organisms/strains | | |
| Wildy-type C57BL/6J mice | The Jackson Laboratory | Strain #000664; RRID:IMSR_JAX:000664 |

(*Continued on next page*)

*Continued*

| REAGENT or RESOURCE | SOURCE | IDENTIFIER |
|---|---|---|
| Software and algorithms | | |
| bowtie2 v2.3.5 | Langmead and Salzberg [64] | N/A |
| cmscan v1.1.14 | Nawrocki and Eddy[65] | N/A |
| Woltka | Zhu et al.[66] | N/A |
| Qiime2 v2021.4 | Bolyen et al.[67] | https://qiime2.org |
| ALDEx2 | Fernandes et al.[24] | N/A |
| MetaCycle | Wu et al.[68] | N/A |
| BIRDMAn[38] | Rahman et al.[38] | N/A |
| DIAMOND v2.1.9 | Buchfink et al.[69] | N/A |
| MZmine v4.1.0 | Schmid et al.[70] | N/A |
| FBMN in GNPS2 | Nothias et al.[71]; Wang et al.[72] | https://gnps2.org |
| Clustal Omega v1.2.4 | Sievers et al.[73] | N/A |
| R v4.4.3 | R Core Team, 2023 | https://www.R-project.org |
| Python v3.6.12 | Python Software, 2023 | http://www.python.org |
| Custom code | This manuscript | Mendeley Data, V1, https://doi.org/10.17632/r3t9jm798y.1 |
| Other | | |
| NovaSeq6000 | Illumina | N/A |
| Q-Exactive Orbitrap mass spectrometer | Thermo Fisher Scientific | Cat# 0726090 |
| 3-in-1 Body Composition Analyzer | EchoMRI | N/A |
| Nova Max Plus glucose meter | Nova Max | N/A |

## EXPERIMENTAL MODEL AND STUDY PARTICIPANT DETAILS

### HFD and TRF animal experiment

A total of 54 8-week-old, wild-type male C57BL/6 mice (Jackson Laboratories, Bar Harbor, ME) were subject to different diet and food access patterns for 8 weeks as previously described.[1] We used male mice as females do not develop DIO or high-fat diet dysmetabolism. Mice were split into three groups: (1) mice fed a normal chow (NCD, LabDiet 5001): 3.36 kcal/gm with ad libitum food access (n = 18, NA), (2) High-fat diet (HFD, TestDiet 58Y1): 5.16 kcal/gm with ad libitum food access (n = 18, FA), or (3) HFD with time-restricted food access (n = 18, FT). Time-restricted food access refers to restricting food access to a period of 8 hours during the dark period (ZT13–21). FT mice were most fasted at ZT13 during the dark phase, while NA and FA mice were most fasted at ZT9 during the light phase. For every 4h time point, three animals from each condition from separate cages were euthanized and cecum samples were collected during a 24h period for each of the 6 timepoints on the Zeitgeber time scale (ZT1, ZT5, ZT9, ZT13, ZT17, ZT21) and stored at -80 °C until further processing. Tissue samples were powderized through mechanical homogenization (mortar and pestle) in liquid nitrogen. We note that six of the FA and FT samples had insufficient RNA yield during nucleic acid extraction processing. This issue arose due to low cecal content from the HFD-fed mice consuming less food by gram, and the high acidity of the cecal environment under HFD conditions interfering with our RNA extraction protocols. Nonetheless, we do not believe this compromises our ability to draw statistically and biologically meaningful conclusions.[74]

### ENB *in vivo* animal experiment

All animals were maintained and used in accordance with the guidelines of the IACUC of the University of California, San Diego. Eight-week-old mice were purchased from Jackson Laboratories and housed in a specific pathogen free facility with a 12h light–12h dark cycle, an ambient temperature of 20–24 °C and humidity of 40–60%. After acclimation for one week, mice were pseudorandomized into four groups based on their initial body weight and body composition and gavaged with 0.2 ml of $1x10^{10}$ CFU/mL EcAZ, EcAZ-$2^{BSH+}$, EcAZ-$1^{DnBSH1}$ or EcAZ-$1^{LgBSH}$. Body weight and food intake were measured every week.

## METHOD DETAILS

### Microbial Engineering

Based on the differential expression results of different BSH genes, we chose 5 *bsh* candidates to engineer into our previously described native *E. coli* chassis with added *cat* resistance and no GFP (referred to here as EcAZ-1-cat).[10] Briefly, all *bsh* genes were codon optimized for *E. coli* expression and placed under the regulation of constitutive promoter J23119. Using CRISPR coupled with homologous recombination, EcAZ-$1^{DnBSH1}$, EcAZ-$1^{DnBSH2}$, EcAZ-$1^{LgBSH}$, EcAZ-$1^{LCAG95BSH}$, and EcAZ-$1^{EpBSH}$ were integrated

at formerly identified *E. coli* Safe Site 9 (SS9).[75] Additionally, each strain had the chloramphenicol acetyltransferase gene, *cat*, integrated at an *attB* site in the genome to allow for strain selection using antibiotics. Correct genomic editing was verified by Sanger sequencing across the site of insertion. Long-read nanopore sequencing of EcAZ-1$^{LCAG95BSH}$ strain confirmed that no off-target edits occurred during the engineering process.

### Bile Acid quantification *in vitro*

The *bsh*-expressing engineered native bacteria were grown in Brain Heart Infusion broth (BHI) at 37 °C overnight, with shaking. After 24h, 1:100 subcultures were inoculated in a 96-deep well plate and incubated at 37 °C with shaking for 4 hours. 10 mM working stocks of bile acids were prepped in 50% methanol (MeOH) (TDCA, TCA, GCDCA, GUDCA), 45% MeOH/10% DMSO (TUDCA, TCDCA), 35% MeOH/30% DMSO (GDCA), or 30%MeOH/40% DMSO (TLCA). 5 mM GLCA was prepared in 25% MeOH/50% DMSO and increased volume of the stock and vehicle were added to final 96-deep well plates for a final 100 μM concentration. 1 mL BHI with 100 μM of each respective bile acid (or vehicle control) was then inoculated in a 96-deep well plate with 10 μL of the subcultured strains. Plates were done in triplicate. Wells were gently mixed using a multichannel pipette and 250 μL of each culture was put in a 96-well plate that was then stored at -80 °C until further processing. The deep well plates were then incubated at 37 °C with shaking for 48 hours, with 250 μL of culture collected and frozen at the 24- and 48-hours marks. Samples were subsequently lysed via 3 rounds of freeze-thaw lysis.

### Bacterial colonization and BSH activity

Feces were collected from mice 6 weeks after one single gavage with the ENBs, then fecal samples were homogenized in 1 ml sterile PBS. Next, homogenized feces from EcAZ colonized mice were either plated on Luria Broth (LB) agar plates containing chloramphenicol (40 μg/mL) to check for unintended bacterial contamination or diluted and plated on LB agar plates containing kanamycin (12.5 μg/mL) to calculate the number of bacteria colonized in the gut. Fecal samples from EcAZ-2$^{BSH+}$, EcAZ-1$^{DnBSH1}$ or EcAZ-1$^{LgBSH}$ colonized mice were plated on LB + chloramphenicol agar plates to calculate the bacterial colonization level. To assess the maintenance of BSH enzyme functionality in the gut, we streaked single colonies from the antibiotic-containing plates on an LB plate containing TDCA, then the white precipitates with colonies and halo surrounding the colonies were evaluated after overnight incubation.

### Blood glucose and insulin quantification

At week 6 after one single gavage with different ENBs, mice were fasted for 16h (Pur-O-Cel bedding) and then orally gavaged with 0.7g sugar/kg body weight of a mixed meal (Ensure, Abbott, Columbus, Ohio). After 0.5 h, postprandial blood glucose was measured by the tail snip using a Nova Max Plus glucose meter. Tail tips were anesthetized with a 5% lidocaine cream (Actavis, Parsippany-Troy Hills, NJ) prior to snip. Postprandial blood was also collected through a submandibular bleed 0.5 h after oral gavage, then centrifuged at 1000 g for 20-30 minutes at 4 °C. Serum was collected, and insulin levels were measured using a mouse ELISA (Crystal Chem Ultra Sensitive Mouse ELISA Kit). This data is deposited in Mendeley Data, V1, https://doi.org/10.17632/r3t9jm798y.1.

### Fat and lean mass quantification

Body composition was measured before ENB treatment and 6 weeks after one single gavage with ENBs. Whole body fat mass and lean mass of live mice were scanned using an EchoMRI™ 3-in-1 Body Composition Analyzer (EchoMRI) with EchoMRI 2022 software.

## QUANTIFICATION AND STATISTICAL ANALYSIS

### 16S data processing

The 16S data was sequenced, cleaned, trimmed and processed as previously described.[1,3] We used the taxon filtered DADA2 processed ASV tables for the diversity analysis.

### Metatranscriptomics sample and data processing

Metatranscriptome sequencing was performed on the mechanically homogenized cecum tissues. Powdered tissue samples were homogenized in TRIzol Reagent (Life Technologies). RNA was isolated with PureLink RNA mini kit (Life Technologies) and rRNA depleted with Ribo-Zero kit (Illumina) according to the manufacturer's instructions. Sample quality control and library preparation were performed by the IGM core at UC San Diego. RNA ScreenTape was used to assess RNA quality and quantity. A sequencing library was obtained based on mRNA. Sequencing was performed on the NovaSeq Illumina platform using 150bp paired-end reads to a mean read count per sample of 71,390,000. All paired reads were cleaned using fastp, trimming 3' polyX and adapter sequence, and using default quality filtering scores and lengths. Mouse reads were removed from the metatranscriptomic data by using bowtie2 v2.3.5 to map to the mouse genome (GRCm38.p5) and removing mapped reads.[64] rRNA and tRNA was then removed from metatranscriptomic data via infernal cmscan v1.1.14 against RFAMs RF00005 (tRNA) and RF00001, RF02541, RF00177 (bacterial rRNA clans) with the parameter –cut_nc to match to the noise cutoff.[65] We aligned the clean reads using bowtie2 v.2.4.5 using the –very-sensitive preset option and ran the alignment against the WoL2 database, the most current and comprehensive version, using the "woltka classify" function in Woltka to get the per genome mapping tables.[66,76] On average 71% of total reads mapped successfully. Followed by collapsing the per genome table using "woltka tool collapse" to pfam functional classifications. To get the genus|

function and species|function tables, we first used ''woltka classify'' with the flag –outmap to get taxonomy mapping information and then ran ''woltka classify'' using –stratify and the outmap file as its input to get the genus and species functional pfam tables. Metatranscriptomic sequences are deposited under ENA project PRJEB89098.

### Metagenomics sample and data processing

DNA was extracted as previously described.[1] Sample quality and quantity was assessed prior to preparation for shotgun metagenomic sequencing. Sample quality control and library preparation were performed by the IGM core at UC San Diego. Sequencing was performed on the NovaSeq Illumina platform using 150bp paired-end reads to a mean read-count per sample of 28,000. All raw paired reads were cleaned, trimmed, filtered in the same way as for the metatranscriptomics. We aligned these raw paired reads using bowtie2 v.2.4.5 using the –very-sensitive preset option and then filtered the.sam files using Zebra Filter for any reads with a coverage threshold below 0.001.[64,77] We then ran the cleaned alignment against the WoL2 database and Woltka in the same way we ran the metatranscriptomics.[66,76] Metagenomic sequences are deposited under ENA project PRJEB89098.

### Diversity analysis

To run the $\alpha$ diversity analysis using the Shannon metric, we rarefied the metatranscriptomics pfam counts table to a depth of 1.4M, metagenomics to a depth of 12000, and 16S to a depth of 6000 on Qiime2.[67] We calculated for the significant differences in $\alpha$ diversity irrespective of collection time using pairwise Man-Whitney U test (two-tailed), FDR corrected using Benjamin-Hochberg at 0.05. To find the effect of condition and collection time on $\alpha$ diversity, we ran the one-way ANOVA model *shannon~condition*zt_time* on each omics method. We supplement this analysis by performing pairwise Student's t-tests (two-tailed), corrected at FDR using Benjamin-Hochberg of 0.05, as a post-hoc test to find differences between the conditions at each collection time point. We tested for normality to perform these parametric tests. As RPCA (robust aitchison distance metric) central log normalizes its input table, we used the non-rarefied counts for the $\beta$ diversity analysis.[78] We ran the PERMANOVA in Qiime2 to find if there were any significant differences in the 16s, metagenomics, and metatranscriptomics $\beta$-diversity by condition and phase.[67]

### Differential expression

The metatranscriptomics pfam counts were TPM normalized before determining the differential expression of each transcript. All the differential pairwise analysis of the diet/feeding conditions by light or dark phase were performed using ALDEx2 with a Welch's t-test and a p-value cut-off of 0.1.[24] To determine if there were significant differences in the number of results determined by metatranscriptomics or metagenomics we used a $\chi^2$ test and p-value cut-off of 0.05. From the significantly different results in the three pairwise group comparisons (FA vs. FT, FA vs. NA, and FT vs. NA), we used venn in R to subset the data further to understand what functions were specific for each comparison. Similarity between groups (e.g., metagenomics vs. metatranscriptomics or Light vs. Dark) was calculated using the jaccard distance matrix. To determine the functional pathways these pfams belong to, we used the pfam-to-go-process.map file from woltka.[66] All plots were generated using ggplot2 on Rstudio.[79]

### Cycling analysis

To determine cycling, we ran the metatranscriptomics and metagenomics TPM normalized pfam tables sub-setted by condition against MetaCycle v.1.2.0 using the JTK_cycle algorithm and a p-value cut-off of 0.05.[68] To determine if there were significant differences in the number of cycling results determined by metatranscriptomics or metagenomics we used a $\chi^2$ test and p-value cut-off of 0.05. We used venn in R to determine what functions overlap and are uniquely cycling among the three conditions. Similarity between metagenomics and metatranscriptomics was calculated using the jaccard distance matrix. All plots were generated using ggplot2 on Rstudio.[79]

### *bsh* expression analysis

To find the per microbe differential expression of *bsh*, we filtered our species|pfam tables for just *bsh* (PF02275). We normalized the transcripts to the housekeeping gene *rpob*, which encodes the beta-subunit of RNA polymerase to find the overall differential expression of *bsh* under the three conditions and two phases using a pairwise Mann-Whitney U test, FDR corrected using Benjamin-Hochberg at 0.05. *rpob* did not show any cycling or diurnal differences modulated by TRF. We then used BIRDMAn, a Bayesian framework for performing differential abundance analysis,[38] to find individual species BSH differences between the three pairwise groups (FA vs. FT, FA vs. NA, and FT vs. NA) in either the light or dark phase. The model we used was a negative binomial model from the SingleFeatureModel class with a beta prior of 5, individual dispersion lognormal prior of 0.5, and 500 iterations. To determine which transcripts had the differential expression patterns of interest, we filtered for transcripts whose 95% high density interval (hdi) had a ratio value range less than 10. Transcripts were considered credible if their hdi did not include an effect size of 0. To perform a targeted search for *bsh*, we aligned the clean reads against a custom database of BSH protein sequences using DIAMOND (v 2.1.9) blastx with default parameters.[69] A custom BSH database was compiled based on amino acid sequences for putative BSHs from the Interpro family IPR029132 (choloylglycine hydrolase, NAAA C-terminal) using the EFI-EST web server in Familes mode.[80] Sequences were manually filtered to those with species-level information available, resulting in a total of 6,638 unique protein sequences. Accession numbers were mapped to amino acid sequences using UniProt ID mapping to compile the database. Quantification of the

abundance of the *bsh* transcripts was performed with the "woltka classify" function in Woltka (v 0.1.5).[66] We then followed the same method to find differential expression for these transcripts and the *bsh* metagenomic genes using BIRDMAn between our pairwise conditions.

### LC-MS/MS sample processing and data acquisition

The lysed samples (about 180 μL) was transferred to a deep 96-well plate and 600 μL of LC-MS grade methanol:water 50:50 v/v was added to each well. The sample plates were sealed with aluminium seal and sonicated for 10 min followed by incubation at -20 °C and then centrifuged for 15 min at 2000 r.p.m. A 200 μL aliquot from each sample's supernatant was transferred to a shallow 96-well plate and the liquid was evaporated in vacuo under centrifugation. The dried extracts were resuspended in 200 μL of 50% methanol:water containing 1 μM sulfadimethoxine as internal standard, mixed thoroughly by pipetting and then sonicated for 15 min. The LC-MS/MS data acquisition was carried out with a Vanquish UHPLC system coupled to a Q-Exactive Orbitrap mass spectrometer (Thermo Fisher Scientific, Bremen, Germany). The chromatographic separation was performed on a Polar C18 column (Kinetex C18, 100 x 2.1 mm, 2.6 μm particle size, 100A pore size – Phenomenex, Torrance, USA), and the mobile phase consisted of $H_2O$ (solvent A), and ACN (solvent B), both acidified with 0.1% formic acid. The LC method consisted of 0-0.5 min 5% B, 0.5-1.1 min 5-25% B, 1.1-7.5 min 25-40% B, 7.5-8.5 min 40-100% followed by a 1.5 min washout phase at 100% B, and a 2.0 min re-equilibration phase at 5% B. The flow rate was set at 0.5 mL/min, the injection volume was fixed at 5 μL, and the column temperature was set at 40 °C. Data-dependent acquisition (DDA) of MS/MS spectra was performed in the positive ionization mode. Electrospray ionization (ESI) parameters were set as: 52.5 AU sheath gas flow, 13.75 AU auxiliary gas flow, 2.7 AU spare gas flow, and 400 °C auxiliary gas temperature; the spray voltage was set to 3.5 kV and the inlet capillary to 320 °C and 50 V S-lens level was applied. MS scan range was set to 150-1500 m/z with a resolution of 35,000 with one micro-scan. The maximum ion injection time was set to 100 ms with an automated gain control (AGC) target of 1.0E6. Up to 5 MS/MS spectra per MS1 survey scan were recorded in DDA mode with a resolution of 17,500 with one micro-scan. The maximum ion injection time for MS/MS scans was set to 150 ms with an AGC target of 5E5 ions. The MS/MS precursor isolation window was set to 1 m/z. The normalized collision energy was set to a stepwise increase from 25 to 40 to 60 with z = 1 as the default charge state. MS/MS scans were triggered at the apex of chromatographic peaks within 2 to 5 s from their first occurrence. The quality and reproducibility of the analyses were evaluated considering the retention time and the m/z of a standard solution containing a mixture of six standards, which was analyzed every 10 samples.

Bile acid annotations and relative quantification using peak area abundances extracted using MZmine 4.1.0 were achieved using Feature Based Molecular Networking (FBMN) on GNPS2 and an expanded set of bile acid libraries.[63,70–72,81] Peak areas for polyamine bile amidates were extracted using Skyline after matching the retention time using synthetic standards.[82] Heatmap and boxplots showing the quantification of the bile acids from the cultures and fecal samples were generated in R using pheatmap and ggplot2.[79,83] Retention time matching was performed by extracting EICs for selected bile acids using the Python pyrawr package and an in-house script deposited on GitHub (https://github.com/wilhan-nunes/raw-xic-export.git). The metabolomic files are deposited in MassIVE under MSV000094578 and MSV000097414 and the GNPS FBMN jobs are https://gnps2.org/status?task=f67a6015e87942fab913beedd63a36aa and https://gnps2.org/status?task=092d720b607e4957ab6b2cd67d15d98f.

### BSH protein sequence characterization

We performed a protein sequence alignment of the BSH proteins we engineered against previously characterized BSHs using Clustal Omega v1.2.4 with default parameters.[44,73] This alignment allowed us to determine phylogeny and protein sequence identity using the UniProt align tool[84] and to identify the location of the glycine- and taurine-preferring motif on the BSH selectivity loop (alignment position 345–347) using the NCBI Multiple Sequence Alignment Viewer v1.25.3.